UC Office of the President
Recent Work

Title
Current Approaches for Investigating and Predicting Cytochrome P450 3A4-Ligand Interactions

Permalink
https://escholarship.org/uc/item/5qq309nq

ISBN
978-3-319-16009-2

Authors
Sevrioukova, Irina F.
Poulos, Thomas L.

Publication Date
2015

Peer reviewed

eScholarship.org Powered by the California Digital Library
University of California

Author Manuscript

Author Manuscript

Author Manuscript

Author Manuscript

HHS Public Access

Author manuscript

Adv Exp Med Biol. Author manuscript; available in PMC 2015 August 11.

Published in final edited form as:

Adv Exp Med Biol. 2015 ; 851: 83–105. doi:10.1007/978-3-319-16009-2_3.

Current Approaches for Investigating and Predicting Cytochrome P450 3A4-Ligand Interactions

Irina F. Sevrioukova and

Department of Molecular Biology and Biochemistry, University of California, Irvine, CA 92697, USA

Thomas L. Poulos

Departments of Molecular Biology and Biochemistry, Chemistry, and Pharmaceutical Sciences, University of California, Irvine, CA 92697, USA

Irina F. Sevrioukova: sevrioui@uci.edu

Abstract

Cytochrome P450 3A4 (CYP3A4) is the major and most important drug-metabolizing enzyme in humans that oxidizes and clears over a half of all administered pharmaceuticals. This is possible because CYP3A4 is promiscuous with respect to substrate binding and has the ability to catalyze diverse oxidative chemistries in addition to traditional hydroxylation reactions. Furthermore, CYP3A4 binds and oxidizes a number of substrates in a cooperative manner and can be both induced and inactivated by drugs. In vivo, CYP3A4 inhibition could lead to undesired drug-drug interactions and drug toxicity, a major reason for late-stage clinical failures and withdrawal of marketed pharmaceuticals. Owing to its central role in drug metabolism, many aspects of CYP3A4 catalysis have been extensively studied by various techniques. Here, we give an overview of experimental and theoretical methods currently used for investigation and prediction of CYP3A4-ligand interactions, a defining factor in drug metabolism, with an emphasis on the problems addressed and conclusions derived from the studies.

Keywords

Cytochrome P450; CYP3A4; Ligand binding; Enzyme inhibition; Drug metabolism; Drug-drug interactions

3.1 Introduction

Cytochrome P450 3A4 (CYP3A4[1]) is one of many human cytochrome P450 (P450) enzymes that plays a central role in drug metabolism.[2] While some P450s specialize in catalyzing very specific reactions (e.g. synthesis of cholesterol or fatty acid oxidation), CYP3A4 biotransforms a wide range of endogenous and exogenous compounds including

Correspondence to: Irina F. Sevrioukova, sevrioui@uci.edu.

[1]*Abbreviations*: *ANF* α-naphthoflavone, *BEC* bromoergocryptine, *BFC* 7-benzyloxy-4-trifluoromethylcoumarin, *BQ* 7-benzyloxyquinoline, b_5 cytochrome b_5, *CPR* NADPH-cytochrome P450 oxidoreductase, *CYP or P450* cytochrome P450.

[2]A review of this scope cannot include all the references pertaining to the subject matter.

Author Manuscript Author Manuscript Author Manuscript Author Manuscript

drugs, toxins and pollutants. This is possible due to a large and malleable active site of CYP3A4 (Fig. 3.1), capable of accommodating substrates varying in size and chemical nature, as well as its ability to catalyze diverse chemical reactions such as alkyl carbon and aromatic ring hydroxylation, *O*- and *N*-dealkylation, and epoxidation [1].

CYP3A4 is also known for atypical (sigmoidal, non-Michaelis-Menten) enzyme kinetics and complex ligand-binding behavior resulting from homotropic and heterotropic cooperativity of some of its substrates. Different categories of atypical kinetic profiles and underlying mechanisms were discussed in detail previously [2–7]. In short, cooperative effects in CYP3A4 are thought to occur when the second (or third) substrate molecule of the same or different nature binds remotely or within the active-site pocket and increases turnover by promoting the productive orientation of the first substrate, which can occur with or without a conformational change in CYP3A4.

Despite substrate promiscuity and a highly plastic active site cavity, CYP3A4 with many substrates displays considerable regio- and stereoselectivity in product formation, indicating that structural features of substrates and/or the active site result in selective substrate binding modes. Another important aspect of CYP3A4-drug interactions is that some drugs as well as natural compounds consumed with food can act as CYP3A4 inhibitors. In vivo, this may lead to drug-drug interactions, perturbed pharmacokinetics and toxicity. There has been a continuous effort to unravel and better understand the CYP3A4 inhibitory mechanisms, the full knowledge of which could help medicinal chemists to develop safer drugs.

Here, we give an overview of experimental and theoretical approaches that have been used for investigation and prediction of CYP3A4-ligand interactions, including absorbance, fluorescence, nuclear magnetic and electron paramagnetic resonance (EPR) spectroscopy, X-ray crystallography, various computational and other techniques. Both soluble and membrane-bound forms of CYP3A4 (liver and insect microsomes, proteoliposomes, lipid bilayer nanodiscs, etc.) have been investigated. Preparation of the protein forms is not discussed in this review but the type of model system used in the experimental work will be specified when necessary.

3.2 Experimental Approaches

3.2.1 Absorbance Spectroscopy

All P450s contain the heme cofactor, whose absorption wavelength (λ_{max}) and amplitude depend on the heme iron oxidation-reduction (redox) and coordination state [8, 9]. The oxidized and reduced ligand-free forms absorb at 415–418 nm and 407–409 nm, respectively. Upon binding in the active site, substrates displace a coordinated water ligand and shift the Soret band to 385–395 nm (type I spectral changes; low- to high-spin shift). Depending on the substrate affinity and spatial fit, the spectral change can be partial or complete. In contrast, molecules that contain unhindered nitrogen atoms can ligate to the heme iron directly or via the axial water molecule, shifting the Soret band to 420–425 nm (type II spectral changes). These compounds usually act as inhibitors but, in some cases, can be metabolized by P450. Finally, the ferrous ligand-free and ligand-bound species can react with carbon monoxide and form a long-lived CO-adduct absorbing at ∼450 nm. Such

Author Manuscript Author Manuscript Author Manuscript Author Manuscript

spectral properties enable researchers to monitor formation and measure affinity of the P450-substrate/inhibitor complexes using conventional and stopped-flow spectrophotometers.

3.2.1.1 Equilibrium Titrations—One parameter reflecting ligand affinity, a spectral dissociation constant (K_s), can be determined from a plot of absorbance changes observed during equilibrium titrations of P450 with a substrate or inhibitor vs. ligand concentration. A hyperbolic fitting is usually satisfactory for weaker ligands, whereas quadratic nonlinear regression is used for strong binders. Two such examples, binding of bromoergocryptine (BEC) and ritonavir to CYP3A4 (K_s of 0.3 μM and 50 nM, respectively), are shown in Fig. 3.2.

Equilibrium titrations could also provide evidence for multiple ligand binding to CYP3A4. If several molecules enter the active site and affect the iron spin equilibrium, then the best fit to the absorbance change vs. [ligand] plot will be a two-site binding (or higher order) hyperbolic equation. The sigmoidal shape of a titration curve, in turn, would be indicative of two cooperative ligand interaction sites. Testosterone is one of the substrates shown to cooperatively bind to two sites in CYP3A4 with the Hill coefficient (n_H) of 1.3 [10, 11]. Positive cooperativity was also detected in the binding of aflatoxin B1 (n_H of 2.3) [12], α-naphthoflavone (ANF; n_H of 1.2–1.7) [11, 13], and Nile Red [NR] (n_H of 1.6) [14]. Acetaminophen and midazolam bind to CYP3A4 with a negative cooperativity [15, 16], whereas progesterone and 7-benzyloxyquinoline (BQ) display both positive and negative cooperativity [10, 17]. Structures of these substrates are shown in Fig. 3.3.

A variation of equilibrium titrations is mixed titrations, when two substrates are added simultaneously at fixed molar ratios. These types of experiments were conducted with testosterone, ANF and nanodisc-incorporated CYP3A4, where the spin shifts caused by the substrates added separately or in mixtures were analyzed [18]. Based on the properties of the two-dimensional spin shift surfaces, it was possible to separate specific heterotropic cooperative interactions from the additive affinities of the two substrates and conclude that the apparent positive heterotropic effect of ANF on testosterone binding is due to an additive spin shift caused by ANF rather than specific favorable ANF-testosterone interactions.

No cooperativity in testosterone and ANF binding was detected using global analysis of equilibrium substrate binding, steady-state NADPH consumption and product formation by nanodisc-incorporated CYP3A4 [19, 20]. Considering the individual testosterone and ANF dissociation constants and fractional contributions of the binding intermediates to the overall enzyme behavior, it was suggested that (1) up to three molecules of each substrate could simultaneously bind to CYP3A4 with little or no cooperativity; (2) the first binding event does not lead to a notable spin-state transition and product formation but accelerates NADPH consumption due to uncoupling; (3) spin shift, product formation and NADPH consumption rates reach maximum when the second substrate molecule binds; (4) association of the third substrate improves coupling efficiency but does not affect turnover rate; and (5) functional cooperativity between substrate molecules underlies cooperativity in testosterone and ANF metabolism observed during steady-state kinetics.

Author Manuscript Author Manuscript Author Manuscript Author Manuscript

If ligands strongly influence heme absorption, normalized instead of simple absorbance difference spectroscopy can be used [13, 21]. In this case, the absorbance amplitude of the low- or high-spin forms of P450 is normalized before changes in other absorption bands are measured. A value related to the equilibrium constant between the high and low spin (K_{spin}) is then determined by subtracting the normalized absorbance of ligand-bound P450 from that of the ligand-free form.

3.2.1.2 Job's Titration and Titration by Dilution—Intensity of light during titration experiments may change with an increase in ligand concentrations (internal filter effect). Job's method of continuous variations and a titration by dilution approach allow one to overcome this problem. Job's method involves absorbance measurements in a series of solutions with a constant total molarity but different protein-ligand ratios. In the titration by dilution experiments, the light path of the sample increases simultaneously with dilution. Both methods were utilized for determination of binding affinity for various CYP3A4 substrates [22–24].

3.2.1.3 Quantitative Spectral Analysis—The principal component analysis technique, also known as bilinear factor analysis and singular value decomposition analysis, was applied for monitoring spin equilibrium in microsomal CYP3A4 at different temperatures and BEC concentrations [25]. Thermodynamic parameters for BEC binding (dissociation constant, ΔH, ΔS and ΔG) and spin transitions in CYP3A4 were evaluated using spectral standards for the high-spin, low-spin and cytochrome P420 (P420) states, leading to a conclusion that the substrate causes profound changes in the protein-heme interactions that favor dissociation of the fifth heme ligand and a low- to high-spin transition.

3.2.1.4 Ligand Binding Kinetics—Individual steps in the ligand-binding reaction can be resolved by stopped-flow spectrophotometry where multi- or single-wavelength kinetic data is collected after rapid mixing of protein and ligand solutions. The CYP3A4-ligand association is usually a complex process that proceeds in several steps [26–31]. The kinetic dissociation constant (K_d) for the CYP3A4-ligand complex can be estimated from a plot of the observed rate constant for the ligand binding reaction (k_{obs} or k_{on}) vs. ligand concentration. In most cases, the K_s and K_d values are close. However, for the CYP3A4-ritonavir complex, the K_d was found to be 17-fold higher than the K_s [28]. To better understand why there was such a big difference between the two related parameters, kinetics of ritonavir binding was reexamined using a wider range of ligand concentrations to include both supra- and sub-equimolar protein:ligand ratios. Under these conditions, the k_{obs} vs. [ritonavir] plot was V-shaped, with a minimum at a protein:ligand ratio of ~1.0 [30], which could arise from ritonavir docking to a peripheral site prior to moving into the active-site cavity.

3.2.1.5 Heme Reduction Kinetics—The P450 heme iron can accept electrons delivered by chemical compounds (e.g. sodium dithionite) or by NADPH via an associated redox partner, NADPH-cytochrome P450 oxidoreductase (CPR). When CO is present in the reaction mixture, heme reduction can be conveniently monitored by following heme-CO adduct formation. Using this approach, it was shown that the electron transfer rate from CPR

Author Manuscript Author Manuscript Author Manuscript Author Manuscript

to purified CYP3A4 is enhanced in the presence of testosterone, Mg^{2+} and cytochrome *b5* (*b*5), but neither of these additives was required for optimal electron transfer in the presence of ethylmorphine (90 % low-spin state) [32]. Differences in the CYP3A4 reduction kinetics measured in human liver microsomes, baculovirus membranes (CPR:3A4 ≈ 8), *E. coli* membranes (CPR:CYP3A4 ≈ 1), a reconstituted system with phospholipids (CPR:3A4 ≈ 2) and a CYP3A4-CPR fusion protein suggested that one regulatory factor may be CYP3A4 clustering/aggregation, as it could create protein pools differing in the electron accepting ability due to spatial or conformational effects [33].

That two types of CYP3A4 oligomers, substrate-sensitive and substrate-insensitive, co-exist under equilibrium was demonstrated by measuring the dithionite-driven reduction of low- and high-spin forms of soluble, nanodisc- and liposome-incorporated CYP3A4 [34]. Another evidence for functional heterogeneity in CYP3A4 was obtained when the flavin domain of cytochrome P450 BM3 was utilized as a redox partner. Only partial heme reduction was observed in soluble CYP3A4 aggregates [35] but complete heme reduction occurred in nanodisc- or liposome-incorporated CYP3A4 monomers [36].

3.2.1.6 CO Rebinding Kinetics—Flash photolysis allows measuring CO recombination kinetics after the CO-Fe bond is disrupted by a laser flash. The CO rebinding kinetics reflects the rate of CO diffusion through the protein matrix and depends on the protein conformation, heme environment and a substrate binding mode. The higher the protein flexibility and the wider the ligand access channel, the higher the CO binding rate. With this methodical approach, it was shown that different CYP3A4 conformers exist [37], and that substrates can accelerate or reduce the CO binding rate by modulating the protein conformation and dynamics [38]. Flavonoids such as ANF, for instance, are thought to enhance the CYP3A4 activity by binding and activating a subpopulation that otherwise is metabolically inactive [39].

3.2.1.7 Heme Depletion Kinetics—Conformation-dependent changes in accessibility of the active site can be analyzed using a heme depletion assay. P450 heme absorbance starts decaying upon addition of an excess of H_2O_2 and can be followed spectroscopically over time. The heme depletion in CYP3A4 is multiphasic, which may result from conformational heterogeneity [40]. Since the rate of the Soret band bleaching depends on the presence of b_5, the assay can also be utilized for investigating CYP3A4-redox partner interactions.

3.2.1.8 High Pressure Spectroscopy—High-pressure spectroscopy can be applied for studying conformational heterogeneity and allosteric mechanisms in CYP3A4 as well [41, 42]. High hydrostatic pressure induces a low-spin shift and a P450-to-P420 conversion in a manner that depends on protein-protein and protein-ligand interactions. Both isolated and microsomal CYP3A4 display barotropic heterogeneity, with no interconversion between the distinct conformers [41]. However, there is no pressure-induced spin shift in microsomal CYP3A4, possibly due to a stabilizing effect of the membrane environment and/or CPR and b_5 that could limit the water access to the active site. In a separate study, a notable difference in the pressure-induced transitions was observed in the presence of allosteric (testosterone and 1-pyrenebutanol) and non-allosteric (BEC) substrates regardless of whether CYP3A4 was in solution or incorporated into a nanodisc. The high- to low-spin shift was complete in

Author Manuscript Author Manuscript Author Manuscript Author Manuscript

the BEC-bound form and partial in the testosterone-and 1-pyrenebutanol-bound P450 [42]. The allosteric substrates were suggested to induce conformational changes that decrease the water flux into the heme pocket and stabilize the high-spin state.

3.2.2 Isothermal Titration Calorimetry (ITC)

ITC titrations, allowing determination of binding stoichiometry based on heat changes, were carried out to estimate how many molecules of BEC and the inhibitor clotrimazol bind to CYP3A4 [26, 27]. Both binding reactions were found to be exothermic, with saturation at an equimolar ligand:CYP3A4 ratio. During ITC titrations, the ligand is usually added to the protein solution. However, owing to limited solubility of BEC and clotrimazol, these compounds were placed into the ITC cell and titrated with CYP3A4.

3.2.3 Equilibrium Dialysis

Ligand binding to CYP3A4 can also be examined by equilibrium dialysis. To determine the stoichiometry of CYP3A4-BEC binding [26], the ligand solution was placed into two cells separated by a dialysis membrane, and CYP3A4 was added to one of the cells. After equilibration, the protein was precipitated and the ligand concentration in both cells was estimated fluorimetrically. The $[BEC_{free}]$ vs. $[BEC_{bound}]$ plot reached a plateau at equal concentrations of BEC and CYP3A4, implying a 1:1 binding stoichiometry.

3.2.4 Inhibitor-Induced Cooperativity

Substrate stoichiometry in CYP3A4 can be estimated based on steady-state kinetics measured in the presence of large inhibitors. Large molecules compete with a substrate which, in turn, affects the Hill coefficient. The n_H value for the BQ debenzylation reaction increased from 1.74 to 2.1–3.7 when bulky troleandomycin, erythromycin, ketoconazole, cyclosporine A or BEC, but not smaller midazolam and testosterone, were present in the reaction mixture, meaning that up to four molecules of BQ can be simultaneously bound to CYP3A4 [43]. The obtained n_H values are still thought to reflect the lower limits of the number of substrate molecules that can enter the CYP3A4 active site.

3.2.5 Fluorescence Spectroscopy

Fluorescent properties of tryptophan residues, substrates, inhibitors and other fluorescent compounds were exploited to investigate protein-ligand interactions, multiple ligand binding sites, and cooperativity in CYP3A4 [14, 26, 27, 44, 45].

3.2.5.1 Fluorescent Substrates—α-Naphthoflavone (ANF) (Fig. 3.3) fluoresces with an excitation wavelength (λ_{ex}) of 320 nm and emission wavelength (λ_{em}) of 440 nm. The fluorescence yield decreases upon ANF ligation to CYP3A4 and, therefore, it was possible to fluorimetrically determine the binding affinity and contribution of ANF to CYP3A4 conformational heterogeneity and substrate cooperativity [23, 26, 46].

The fluorescent properties of bromoergocryptine (BEC) (λ_{ex} = 320 nm; λ_{em} = 440 nm; Fig. 3.4) were utilized to resolve a multi-step ligand binding process. Comparison of BEC-dependent fluorescence and absorbance changes observed during interaction with CYP3A4

Author Manuscript Author Manuscript Author Manuscript Author Manuscript

enabled the detection of an 'absorbance-silent' step, attributed to substrate association to a peripheral site prior to translocation into the active-site cavity [26].

The fluorescent properties of NR (λ_{ex} = 550 nm; λ_{em} = 620 nm; Fig. 3.3) helped identify two-site binding to CYP3A4 [45] and probe allostery and sequential metabolism [14, 47]. Similar to testosterone and ANF [13, 21], NR has a minor effect on the heme spin-state equilibrium when it binds to a high-affinity site (K_d of 0.3 μM), whereas its association to a low-affinity site (K_d of 2.2 μM) leads to the majority of the ligand-induced spin shift [45].

Based on differences in the fluorescence emission of monomers and dimers of pyrene (λ_{ex} = 295 nm; $\lambda_{em}^{monomer}$ = 370–390 nm; λ_{em}^{dimer} = 480 nm; Fig. 3.4), it was shown that two pyrene molecules bind simultaneously in the CYP3A4 active site and that a π-π stacked pyrene-pyrene complex rather than a single monomer undergoes oxidation [44].

3.2.5.2 Fluorescent Products—7-Hydroxy-4-trifluoromethylcoumarin (λ_{ex} = 410 nm; λ_{em} = 538 nm) is formed upon CYP3A4-dependent debenzylation of 7-benzyloxy-4-trifluoromethylcoumarin (BFC). BFC is widely used for rapid fluorimetric measurements of CYP3A4 activity and detection of drug-drug interactions in conventional and high-throughput screening assays.

7-Hydroxyquinoline (λ_{ex} = 410 nm; λ_{em} = 538 nm) is the product formed upon BQ debenzylation. In the inhibitory assays, BQ was shown to be a less sensitive fluorimetric probe than BFC [48].

3.2.5.3 Fluorescent Inhibitors—Several fluorescent inhibitors specific for CYP3A4 have been synthesized by attaching a dansyl, deazaflavin or pyrene group to the C6 atom of testosterone [49]. Fluorescence of steroid derivatives is quenched upon reaction with the heme but can be restored when the activesite-bound fluorophore is displaced by another compound, which makes possible fluorimetric determination of relative affinities of various compounds and monitoring of drug-drug interactions.

3.2.5.4 Fluorescent Probes—2-*p*-Toluidinylnaphthalene-6-sulfonic acid (TNS) (λ_{ex} = 320 nm; λ_{em} = 440 nm) is non-fluorescent in aqueous solutions but emits light in a hydrophobic environment, such as the protein interior. Upon binding to CYP3A4, TNS induces type II spectral changes and fluoresces with a high quantum yield [50]. Based on changes in steady-state and time-resolved TNS fluorescence, it was suggested that a remote, high-affinity binding site for TNS exists, occupation of which could affect the active-site environment.

6-(Bromoacetyl)-2-(dimethylamino)naphthalene (BADAN; λ_{ex} = 387 nm, λ_{em} = 520 nm), 7-(diethylamino)-3-(4′-maleimidylphenyl)-4-methylcoumarin (CPM; λ_{ex} = 405 nm, λ_{em} = 530 nm) and monobromobimane (mBBr; λ_{ex} = 395 nm, λ_{em} = 490 nm) are environment-sensitive thiol-reactive fluorescent probes used for studying the interaction between cysteine-depleted CYP3A4 (only Cys58 and/or Cys64 left) and several substrates that do or do not display binding cooperativity [51]. Analysis of the substrate- and probe-dependent fluorescence changes and H_2O_2-induced heme destruction kinetics provided evidence for a

Author Manuscript Author Manuscript Author Manuscript Author Manuscript

distinct low-affinity ANF binding site, association to which is not accompanied by a heme spin shift. BADAN-labeled CYP3A4 was also used for investigating the effects of reduced glutathione (GSH) on BFC and BQ oxidation [52]. GSH eliminates homotropic cooperativity of BFC and BQ but amplifies the activating effect of ANF on BFC oxidation, and is suggested to have two binding modes, one of which is direct coordination to the heme iron via the SH-group.

3.2.5.5 Single Molecule Fluorescence Spectroscopy—Single molecule fluorescence studies were conducted on nanodisc-incorporated CYP3A4 where the evanescent NR excitation, generated using internal reflection fluorescent microscopy, was followed by measurements of residence times in the low-occupancy NR-bound complexes [47]. The observed biphasic dwell-time distribution is thought to reflect two phases of the NR dissociation reaction: a fast off-rate from the nanodisc lipid bilayer and a slow off-rate from the protein (30 and 1.5 s^{-1}, respectively). Based on a fivefold ANF-induced decrease in the slow phase of NR dissociation, it was concluded that the CYP3A4 effectors could modulate the substrate off-rates by altering structure/dynamics of monomeric CYP3A4.

3.2.6 Fluorescence Resonance Energy Transfer (FRET)

FRET is a mechanism through which energy is transferred between two closely positioned fluorophores. If the distance is short enough, an excited donor can transfer energy to an acceptor through nonradiative dipole-dipole coupling. FRET efficiency, therefore, can serve as a measure of a distance between two fluorophores. FRET between BEC, 1-pyrenemethylamine (λ_{ex} = 340 nm; λ_{em} = 380 nm) or PB (λ_{ex} = 331 nm; λ_{em} = 380 nm) and the CYP3A4 heme was utilized in combination with absorbance spectroscopy to monitor individual ligand-binding events [22–24]. Unlike BEC and 1-pyrenemethylamine that bind to a single site in CYP3A4, association of 1-pyrenebutanol was consistent with a two-step sequential model, where the spin transition takes place upon 1-pyrenebutanol binding to a low-affinity site [22]. In the F213W, F304W and L211F/D214E mutants, however, cooperativity in 1-pyrenebutanol binding was altered and a partial spin shift was observed in the binary rather than ternary enzyme-substrate complex [24]. In another study, substrate-dependent conformational transitions in CYP3A4 were analyzed by measuring FRET from the BADAN and CPM labels to the heme, and from tryptophan residues to BADAN [51]. Finally, a FRET-based assay employing *N*-(4,4-difluoro-5,7-dimethyl-4-bora-3α,4α-diaza-*s*-indacene-3-yl)methyliodacetamide (BODIPY-FL iodoacetamide) was utilized for testing how the surface density of liposome-bound CYP3A4 affects spin equilibrium and heme reduction kinetics [36].

3.2.7 Luminescence Resonance Energy Transfer (LRET)

LRET uses the long-lived triplet state of a phosphorescent probe as an energy donor. Its advantage over FRET is the longer distance at which the energy can be transferred and the longer donor life-time, which makes LRET measurements more accurate and orientation independent. Using an LRET-based method, the relation between the concentration of membrane-bound CYP3A4 and its oligomeric state was examined [46]. Cysteine-depleted CYP3A4 was labeled with either erythrosine 5′-iodacetamide (ERIA) or DY-731 maleimide (DYM), serving as a LRET donor and acceptor, respectively. Addition of CYP3A4-DYM to

Author Manuscript Author Manuscript Author Manuscript Author Manuscript

CYP3A4-ERIA-containing liposomes led to a drastic decrease in the donor emission and delayed fluorescence of the acceptor. The sigmoidal dependence of the LREP amplitude on the surface density of liposomal CYP3A4 became hyperbolic in the presence of ANF. This finding and a correlation between the oligomerization state of CYP3A4 and its susceptibility to activation by ANF support the hypothesis that protein-protein interactions can play a role in the allosteric mechanism.

3.2.8 Photoaffinity Labeling

Protein labeling with photoaffinity probes can provide information on the substrate recognition sites without carrying out the enzymatic reaction. The method utilizes a labeling reagent that upon photolysis converts to an extremely reactive intermediate and covalently binds to the activesite residues. Chromene-like molecules act as photoaffinity ligands for CYP3A4 [53, 54]. Upon UV light irradiation, these compounds rearrange into conjugated tricyclic structures with different life-times. Plant benzochromene, lapachenole, serves as a substrate and a competitive inhibitor of CYP3A4 but when photoactivated, it becomes an irreversible inactivator and fluorescently modifies thiol groups of cysteine residues (Fig. 3.5) [53]. Analysis of the lapachenole-linked protein identified Cys98 and Cys468 as the primary modification sites [54]. The functional role of the surface Cys468 remains unclear, whereas Cys98 is part of the substrate access channel and, hence, could affect substrate recognition and catalysis.

3.2.9 Circular Dichroism (CD) Spectroscopy

CD spectroscopy allows rapid determination of the secondary structure and folding properties of proteins and, in conjunction with other methods, was used for investigation of CYP3A4 inhibition by Cu^{2+} and Zn^{2+} ions [55, 56]. One of the inhibitory effects of Cu^{2+} on testosterone hydroxylation was induction of a conformational change in CYP3A4 (7 % decrease in the α-helix content) [55]. Zn^{2+}, on the other hand, had not only a more pronounced effect on CYP3A4 secondary structure (11 % decrease in α-helix content) but also prevented the stimulatory action of b_5 on testosterone metabolism [56]. Thus, the cytosol metal ion balance could be one of the factors regulating CYP3A4 activity in vivo.

3.2.10 Linear Dichroism (LD) Spectroscopy

LD is observed when plane-polarized light is absorbed by samples that are oriented intrinsically or by external forces. With this spectroscopic technique, information on the orientation of a chromophore or structures within molecules can be obtained. LD measurements were performed to characterize the heme tilt angle in nanodisc-incorporated CYP3A4 [57]. A low deviation between experimental values (average of 59.7 ± 4.1°) indicated that CYP3A4 is specifically orientated relative to the lipid bilayer.

3.2.11 Surface Plasmon Resonance (SPR)

SPR on metallic surfaces is a powerful optic sensing method for monitoring label-free bimolecular interactions. SPR analysis was utilized to investigate CYP3A4 binding to antifungal azoles, itraconazole and ketoconazole [58]. Based on the binding kinetics, absorbance spectroscopy and catalytic studies, two orientation modes for both drugs were

Author Manuscript Author Manuscript Author Manuscript Author Manuscript

identified: a catalytically productive mode and a slowly dissociating inhibitory mode. In combination with other methods, the SPR technique was used to determine the off-rates for structurally related quinolone carboxamide compounds acting as type I and type II ligands of CYP3A4, and helped to clarify the kinetic mechanism for their metabolism [59].

A related method, SPR in nanometer-sized structures or localized SPR (LSPR) that also depends on the refractive index of the surrounding media, was developed for detection of CYP3A4-drug interactions [60]. Nanodisc-bound CYP3A4 was covalently immobilized on the surfaces of silver nanoparticles and the drug binding was monitored by measuring the resonant coupling between the nanoparticles and the CYP3A4 heme. Ligand-induced changes in position and amplitude of the LSPR spectrum maxima correlated well with the spectral changes observed in solution.

3.2.12 Nuclear Magnetic Resonance (NMR)

NMR T_1 paramagnetic relaxation studies provided the first physicochemical evidence for the allosteric substrate binding in the CYP3A4 active site [15, 61, 62]. T_1 relaxation experiments are suited for analyzing CYP3A4 allosterism because they allow determination of distances from a paramagnetic center (the heme iron) to the protons of multiple substrates and, hence, can detect changes in their relative orientation. One NMR study investigated heterotropic cooperativity between midazolam and two effectors, testosterone and ANF [61]. Midazolam is hydroxylated at C1′ and C4′ positions, and the ratio between metabolite formation rates depends on midazolam concentration and the presence of testosterone or ANF. Owing to negative homotropic cooperativity, the 1′-hydroxyproduct is preferably formed at low midazolam concentrations, whereas the 4′-hydroxylation rate increases at higher substrate concentrations [16]. The midazolam protons-heme distances measured in the absence and presence of the effectors suggest that midazolam can rotate within the active site or slide parallel to the heme plane [61]. The NMR data also indicate that ANF and testosterone exert their allosteric effects through direct binding in the vicinity of the heme and by reorienting midazolam, to bring the C1′ or C4′ atoms closer to the heme, which explains the kinetics of activation and preferable formation of 1′-hydroxy- and 4′-hydroxymidazolam in the presence of ANF and testosterone, respectively.

In combination with the molecular docking technique, T_1 longitudinal NMR relaxation was applied to probe the cooperativity of midazolam metabolism with carbamazepine serving as a heterotropic effector [62]. Similar to testosterone, carbamazepine inhibits formation of 1′-hydroxymidazolam and, as this study revealed, assumes a stacked configuration with midazolam and brings its C4′ atom closer to the heme. Stacking of two midazolam molecules gives the same result, whereas a single midazolam docks with the C1′ atom closest to the heme. Since many CYP3A4 substrates have a planar aromatic structure, ligand cooperativity through direct stacking interactions was proposed to be one of the possible allosteric mechanisms.

Using NMR T_1 paramagnetic relaxation, positioning of two other substrates, acetaminophen and caffeine, in the CYP3A4 active site was investigated [15]. CYP3A4-dependent acetaminophen oxidation exhibits negative homotropic cooperativity ($n_H = 0.7$) but follows Michaelis-Menten kinetics in the presence of caffeine. The calculated distances were

Author Manuscript Author Manuscript Author Manuscript Author Manuscript

consistent with acetaminophen coordination to the heme through the amide group. Upon entering the active site, caffeine is thought to disrupt the weak Fe-N coordination, thereby promoting acetaminophen oxidation. However, it remains unclear whether caffeine, more remote from the heme than acetaminophen, directly interacts with acetaminophen and precludes its coordination or affects the active-site conformation leading to acetaminophen reorientation.

A magic-angle spinning solid-state NMR (MAS SSNMR) spectroscopic study on ^{13}C, ^{15}N-enriched nanodisc-incorporated CYP3A4 demonstrated its structural integrity and proper folding [63]. Analysis of the BEC binding reaction showed that CYP3A4 remains fully active after precipitation with polyethylene glycol, required for SSNMR measurements. Despite good quality, 2D MAS SSNMR spectra were not sufficient for determining site-specific assignments.

3.2.13 Electron Paramagnetic Resonance (EPR) Spectroscopy

Testosterone-dependent spin state equilibrium in CYP3A4 was compared by EPR and optical spectroscopic titrations [21]. To quantify and characterize the single and double occupancy testosterone binding sites, the protein concentration in two sets of experiments either exceeded or was below the K_d for testosterone. Using this combined approach, it was possible to construct a free energy landscape for multiple ligand binding, which suggested that the first testosterone binds with a higher affinity to a ‘non-productive’ site, whereas the second testosterone displaces the bound water and drives the heme to the high-spin state more efficiently than the first.

EPR and UV-vis spectroscopy were also used to examine heterotropic cooperativity and individual binding events for ANF and testosterone [13]. Two types of binding sites for both substrates were identified: high-affinity spinstate insensitive (peripheral) and lower-affinity spin-state sensitive (proximal, near the heme). Based on the thermodynamic analysis of the testosterone- and ANF-induced spin shifts, testosterone was proposed to bind to CYP3A4 sequentially and occupy the proximal site after the peripheral site is saturated. It was speculated also that testosterone affinity for the proximal site increases upon a conformational change caused by ANF association to the peripheral site.

A combination of conventional continuouswave and pulsed EPR (hyperfine sublevel correlation spectroscopy (HYSCORE)) techniques helped to investigate and compare the binding mechanism of 1,2,3-triazole and 17α-(2H-2,3,4-triazolyl)estradiol [64]. Although both compounds are type II ligands of CYP3A4, they induce different perturbations in the EPR *g* values and, as the HYSCORE analysis showed, the 1,2,3-triazole moiety does not displace the axial water molecule when incorporated into the 17α-estradiol scaffold. Instead, 17α-(2H-2,3,4-triazolyl)estradiol hydrogen-bonds to the coordinated water ligand and, by altering its field strength, causes the spin-state change. This study raises concerns on interpreting the P450-ligand structure based on optical spectra, as some ligands that produce type II spectral changes are not always directly ligated to the heme.

Author Manuscript Author Manuscript Author Manuscript Author Manuscript

3.2.14 Resonance Raman (RR) Spectroscopy

RR spectroscopy was applied to identify substrate- and redox-dependent structural changes in nanodisc-incorporated CYP3A4 [65]. Analysis of the high and low frequency RR spectra of ligand-free and BEC-, testosterone- or erythromycin-bound CYP3A4 led to a conclusion that the size and number of substrate molecules bound have no significant effect on the ferric heme structure but greatly influence the conformation of gas ligands (CO and O_2) and the ferrous heme structure. In particular, BEC and testosterone induce changes in the low frequency RR spectrum associated with the heme peripheral group dispositions or out-of-plane macrocycle distortion, which could have an impact on the reactivity of intermediates and CYP3A4 function.

3.2.15 Isotope Fractionation (Kinetic Isotope Effect)

Deuterium-containing substrate analogs were used for examining the mechanism of CYP3A4-dependent ezlopitant dehydrogenation and testosterone hydroxylation [66, 67]. Ezlopitant is metabolized to a benzyl alcohol and a benzyl alkene, where the latter is formed directly rather than via sequential dehydration of the benzyl alcohol. When deuterium was incorporated into the benzylic position, a low isotope effect (ratio between the reaction rate constant of the light and heavy isotope) was observed for both products, indicating that benzylic hydrogen abstraction is obligatory in the formation of both metabolites and there is no metabolic switching (change in regional specificity of ezlopitant metabolism). However, placement of deuterium atoms at adjacent positions led to a small inverse isotope effect on benzyl alcohol but not alkene formation. This suggested that formation of the alkene requires benzylic hydrogen abstraction and that the benzylic radical partitions between the formation of the two metabolites.

Analysis of metabolites of ^{2}H- and ^{3}H-labeled forms of testosterone showed that the testosterone 6β-hydroxylation reaction is stereoselective, as CYP3A4 abstracts hydrogen and rebounds oxygen only at the β-face [67]. A high intrinsic isotope effect (^{D}k of 15) for the labeled testosterone 6β-hydroxylation was consistent with the initial hydrogen atom abstraction. In non-competitive reactions, some metabolic switching occurred and the ^{D}k value was attenuated (<3). Because considerable attenuation in ^{D}k was also observed for BQ *O*-debenzylation, the C-H bond breaking reaction is unlikely to be rate-limiting.

3.2.16 Isotope Dilution Analysis

Sequential NR metabolism and heterotropic allosteric activation by ANF were investigated by isotope dilution analysis to quantitatively measure the relative flux of a reactive cycle intermediate [68]. NR is metabolized by CYP3A4 to monodesethyl-NR (M1), which is sequentially oxidized to didesethyl-NR (M2) (Fig. 3.6). Comparison of metabolites produced by effector-free and ANF-bound CYP3A4 upon incubation with a mixture of deuterated NR and unlabeled M1 suggested that ANF increases the velocity of M1 and M2 production, and modulates the branching k_{cat}/k_{off} ratio in favor of M2 by affecting the substrate off-rate.

Author Manuscript Author Manuscript Author Manuscript Author Manuscript

3.2.17 Electrochemistry

Replacement of the natural electron delivery system, a CPR/NADPH redox pair, by an electromotive force is one of the approaches for developing biosensors for rapid monitoring of CYP3A4-mediated drug metabolism. Purified CYP3A4 was immobilized on gold electrodes coated with 3-mercapto-1-propenesulfonic acid [69], carbon nanofibers [70] and glassy carbon electrodes modified with poly(diallyldimethy-lammonium chloride [71] or Nafio-cobalt (III) sepulchrate [72], whereas CYP3A4-containing didodecyldimethylammonium bromide vesicles were attached to a platinum disc electrode [73]. Thiolate-coated gold electrodes, in turn, were used for immobilization of hepatic microsomes [74]. Using these systems, it was possible to monitor CYP3A4-drug interactions, drug metabolism and inhibition reactions.

Cyclic voltammograms of immobilized CYP3A4 have two peaks attributed to the Fe^{+3}/Fe^{2+} redox couple. When a substrate and oxygen are present, heme reduction is coupled to substrate oxidation, manifested as an increase in the cathodic peak current. The surface concentration of an electro-active enzyme (n) is estimated based on the Faraday's Law: $Q = nF$, where F is the Faraday's constant and Q is the total charge transferred upon reduction of CYP3A4. Q is calculated from the integration of the reduction peak recorded under anaerobic conditions, whereas the enzyme turnover is estimated based on n and the substrate-dependent catalytic current measured by chronoamperometry.

Electrode-immobilized CYP3A4 metabolizes drugs similar to the microsomal protein, with comparable product formation rates and small contribution of H_2O_2 to the catalytic cycle [69]. The electrochemically-driven CYP3A4 reactions are sensitive to the substrate concentration and can be inhibited by ketoconazole, cimetidine and diclofenac [69, 71], which enables estimation of the k_{cat} and K_m values for the substrate turnover and IC_{50} for the inactivators (a concentration of an inhibitor that reduces substrate metabolism by 50 %). Some biosensors were reported to have a rapid response time and ability to detect very low concentrations of drugs and pollutants and, hence, could be utilized for electrochemical detection in biological samples [72, 73].

3.2.18 Chemical Auxiliary Approach

A chemical auxiliary was utilized to control the selectivity of CYP3A4 reactions [75]. By linking substrates to inexpensive, achiral, cell-permeable theobromine, it was possible to achieve predictable stereo- and chemoselective hydroxylation and epoxidation at the fourth carbon from the auxiliary (Fig. 3.7). The method is limited to substrates that are not larger than theobromine, but the advantage is that it does not yield overoxidation products and is tolerant to various functional groups.

3.2.19 X-ray Crystallography

X-ray crystallography provides direct insights into the protein structure and protein-ligand interactions. Recombinant mammalian P450s can be crystallized upon deletion of the membrane-binding fragment and, in some cases, modification of the N-terminus [76]. Multiple CYP3A4 crystal structures have been solved recently but mostly with type II inhibitors bound [28–31, 77–80]. Obtaining co-crystals of CYP3A4 with substrates is

Author Manuscript Author Manuscript Author Manuscript Author Manuscript

challenging because they dissociate from the active site during crystallization. Thus far, only BEC- and erythromycin-bound structures are available, where only BEC is bound in a productive mode [29, 79].

Inhibitors co-crystallized with CYP3A4 include metyrapone, ketoconazole, ritonavir, desthiazolylmethyloxycarbonyl ritonavir and seven desoxyritonavir analogs (GS2-GS8) that widely vary in K_d (22 nM–4 μM) [28–31, 77, 79, 80]. Interestingly, the ketoconazole-, GS4- and GS5-bound structures contain two inhibitor molecules bound to the active site: ketoconazole1 and ketoconazole2 associate in an antiparallel tandem fashion, GS5-1 and GS5-1 in an intertwined parallel mode, and GS4-1 and GS4-2 in a perpendicular mode (Fig. 3.8). Thus, X-ray data proves that multiple molecules differing in size and chemical nature can simultaneously bind to CYP3A4. Comparison of the binding affinity, IC_{50} and orientation modes of ritonavir-like compounds (reviewed elsewhere [81]) helped to better understand the inhibitory mechanism and derive a pharmacophore for a CYP3A4-specific inactivator that could guide structure-based inhibitor design (Fig. 3.9).

Another interesting finding was a peripheral sterol binding site in the CYP3A4-progesterone structure [77]. Instead of associating to the active site, progesterone was found to dock 17Å away from the heme in a surface hydrophobic pocket comprised by the F′-G′-loop residues. Since progesterone displays both negative and positive binding cooperativity [10, 17], it was hypothesized that the progesterone-binding pocket represents a peripheral site where hydrophobic substrates associate before moving into the active-site cavity.

When all available X-ray models of CYP3A4 are superimposed, it becomes evident that very little structural change is needed to accommodate bulky and structurally diverse compounds, even two at a time. Conformational changes take place primarily in the F-G- and C-terminal loop regions, the I-helix adjacent to the heme, and the 369–371 peptide (Fig. 3.10). Such local and minor rearrangements argue against the conformational-heterogeneity-driven allostery in CYP3A4 and rather support the multiple substrate binding mechanism without major conformational changes, as proposed for P450eryF [82].

3.3 Computational Approaches

Because X-ray crystallography has its limitations and co-crystallization of CYP3A4 with the compound(s) of interest is not always possible, theoretical studies are more frequently used these days to investigate the dynamics of ligand binding and catalytic mechanism, predict ligand association modes, and identify substrate and solvent channels. Moreover, computer modeling techniques are indispensible for prediction of CYP3A4-mediated drug metabolism and drugdrug interactions, some of which will be briefly described in this section.

3.3.1 Molecular Dynamics (MD) Simulations

One of the principal tools to theoretically study biological molecules is MD simulations that derive time-dependent dynamic behavior and give a view of the atomic motions. In combination with other approaches, MD simulations were conducted on CYP3A4 in a number of studies, which (1) suggested that the F-F′-loop (residues 211–218) defines the promiscuity and broad substrate selectivity of CYP3A4 [83], and Ser119, Phe205, Arg212,

Author Manuscript Author Manuscript Author Manuscript Author Manuscript

Phe213 and Phe304 are key residues that help orient substrates in the active site [47, 83–86]; (2) identified preferred substrate access/egress and solvent channels [87–90]; (3) clarified the mechanism of cooperative binding of diazepam and ketoconazole [84, 91] and the role of CPR in activating water channels [92]; and (4) characterized the membrane-bound state of CYP3A4 [57, 93, 94].

In steered MD (SMD), a harmonic restraining potential is applied to a protein or ligand in order to manipulate the ligand by pulling it along desired degrees of freedom. SMD with adaptive direction adjustments is an improved method that could accelerate MD simulations, find optimal pathways for ligand dissociation, and bypass a barrier along the failed direction. This method was used to investigate dissociation of the CYP3A4-bound inhibitor metyrapone and led to the discovery of a pathway with a lower energy barrier, shorter dissociation time and shorter motion trajectory compared to those predicted by conventional SMD [95, 96].

3.3.2 Quantum Mechanics/Molecular Mechanics (QM/MM) and Density Functional Theory (DFT) Calculations

A hybrid QM/MM approach is a molecular simulation method for studying chemical processes in solution and in proteins, whereas DFT is a quantum mechanical modeling method for electronic structure calculation by using functionals of the spatially dependent electron density. Theoretical calculations were applied to CYP3A4 to estimate the activation energy of the intermediate formation and predict the binding modes for indapamide and 4-aminopiperidine [85, 86], investigate interaction between nevirapine, carbamazepine and endogenous steroids [97], explore features of the catalytic oxyferryl species (compound I) [98], model the regioselectivity preference of testosterone hydroxylation [99], and test the reactivity of various sites on flunitrazepam and progesterone [100].

Reaction dynamic calculations for the testosterone 6β-hydrogen/deuterium abstraction were performed at the level of canonical variational transition state theory with a multiconfigurational MM technique, allowing the construction of a semiglobal full-dimensional potential energy surface, to gain deeper insights into the quantum tunneling in testosterone hydroxylation by CYP3A4 [101]. In agreement with the experimental results [67], the calculated multidimensional tunneling coefficients indicated substantial contributions by quantum tunneling which, however, only modestly contributed to the kinetic isotope effects. The use of a gas-phase model without considering the protein-solvent interactions was suggested to be one of the reasons for the discrepancy between the theoretical and experimental results.

Gas phase DFT calculations were also conducted to examine the binding of unsubstituted imidazole, 1,2,4- and 1,2,3-triazole to a model Fe^{3+} heme in an attempt to understand underrepresentation of the latter functional group among P450 inhibitors [64]. It was found that 1,2,3-triazole interacts with the heme weaker than other azoles, ligates to heme iron with either N1 or N2 atoms, and forms a longer Fe^{3+}-N bond due to lower basicity.

The binding free energies of 16 structurally diverse CYP3A4 inhibitors to the iron porphyrin model, calculated using DFT and the implicit solvation methods in water, were shown to be

Author Manuscript Author Manuscript Author Manuscript Author Manuscript

a good descriptor in interpreting the CYP3A4-inhibitor interaction [102]. The relative free energies in the gas phase were mainly responsible for the total binding free energies in water, although desolvation could affect the inhibitor affinity.

3.3.3 In Silico Drug Metabolism Prediction

Computational techniques are indispensable and increasingly used in early drug design along with in vitro methods to predict substrate affinity, liability and metabolic pathways. Before the X-ray structure of CYP3A4 became available, homology modeling, quantitative structure-activity relationship (QSAR) modeling and building a 3D-pharmacophore were utilized for drug metabolism prediction [103]. Pharmacophore modeling requires a large and rigid template to identify structural determinants (conformation, shape and electronic properties) of substrates, inhibitors or metabolites critical for catalytic specificity, which could indirectly provide information on the protein active site. QSAR modeling, in turn, is applied to large datasets of molecules and molecular descriptors to derive 3D-features of substrates and inhibitors that can interact with a specific enzyme. Both approaches generated useful information about CYP3A4. In particular, they helped develop pharmacophores for substrates and inhibitors [104–109] and suggested that hydrophobicity and hydrogen bonding are dominant factors guiding ligand binding [104, 107, 110]. Semi-empirical AM1 molecular orbital calculations of the energy of hydrogen radical abstraction is another modeling approach that can predict likely sites of CYP3A4-mediated metabolism by relying solely on the electronics and inter-molecular sterics of drug-like molecules [111].

QSAR modeling is still used in the pharmaceutical industry to analyze very large high-throughput screening sets and to predict CYP3A4 inhibition and substrate potential. Owing to recent structural and computer modeling advances, QSAR methodology was utilized in combination with the multiple pharmacophore hypothesis approach [112], advanced docking techniques (MetSite, GLUE, AutoDock and other) [113–116], GALAS (Global Adjusted Locally According to Similarity) method [117, 118], structure-based comparative molecular field analysis [119], and NMR spectroscopy data [120]. Gaussian kernel weighted *k*-nearest neighbor models were also used for in silico prediction of CYP3A4 inhibitors [121]. Accuracy, sensitivity and specificity of some of the modeling methods were recently compared [118, 122, 123]. The modern and most powerful approach for predicting drug metabolism and drug-drug interactions is a combination of structure-based docking, MD and quantum chemical calculations, which is reviewed elsewhere [124].

3.4 Conclusions

Owing to a central role of CYP3A4 in drug metabolism, it is crucial to fully understand the mechanism of CYP3A4-ligand interactions. In this review, we summarized methodical approaches currently used in the CYP3A4 research, highlighting the problems addressed and conclusions made in relevant studies. Although utilization of a wide array of biochemical, biophysical, structural and computational techniques led to breakthroughs in our understanding of how CYP3A4 functions, some of the processes, such as substrate cooperativity and the mechanism of drug-drug interactions, still need to be clarified. Future

Author Manuscript Author Manuscript Author Manuscript Author Manuscript

development and employment of new methodologies to the CYP3A4 research could lead to new discoveries that may help resolve these issues.

Acknowledgments

Financial support from the National Institute of General Medical Sciences (Grant GM57353) and the California Center for Antiviral Drug Discovery is gratefully appreciated.

References

1. Rendic S, Di Carlo FJ. Human cytochrome P450 enzymes: a status report summarizing their reactions, substrates, inducers, and inhibitors. Drug Metab Rev. 1997; 29:413–580. [PubMed: 9187528]
2. Atkins WM, Wang RW, Lu AY. Allosteric behavior in cytochrome P450-dependent in vitro drug-drug interactions: a prospective based on con-formational dynamics. Chem Res Toxicol. 2001; 14:338–347. [PubMed: 11304120]
3. Hutzler JM, Tracy TS. Atypical kinetic profiles in drug metabolism reactions. Drug Metab Dispos. 2002; 30:355–362. [PubMed: 11901086]
4. Atkins WM. Non-Michaelis-Menten kinetics in cytochrome P450-catalyzed reactions. Annu Rev Pharmacol Toxicol. 2005; 45:291–310. [PubMed: 15832445]
5. Sligar SG, Denisov IG. Understanding cooperativity in human P450 mediated drug-drug interactions. Drug Metab Rev. 2007; 39:567–579. [PubMed: 17786639]
6. Davydov DR, Halpert JR. Allosteric P450 mechanisms: multiple binding sites, multiple conformers or both? Expert Opin Drug Metab Toxicol. 2008; 4:1523–1535. [PubMed: 19040328]
7. Denisov IG, Sligar SG. A novel type of allosteric regulation: functional cooperativity in monomeric proteins. Arch Biochem Biophys. 2012; 519:91–102. [PubMed: 22245335]
8. Jefcoate CR. Measurement of substrate and inhibitor binding to microsomal cytochrome P-450 by optical-difference spectroscopy. Methods Enzymol. 1978; 52:258–279. [PubMed: 209288]
9. Schenkman JB, Sligar SG, Cinti DL. Substrate interaction with cytochrome P-450. Pharmacol Ther. 1981; 12:43–71. [PubMed: 7019934]
10. Harlow GR, Halpert JR. Analysis of human cytochrome P450 3A4 cooperativity: construction and characterization of a site-directed mutant that displays hyperbolic steroid hydroxylation kinetics. Proc Natl Acad Sci U S A. 1998; 95:6636–6641. [PubMed: 9618464]
11. Hosea NA, Miller GP, Guengerich FP. Elucidation of distinct ligand binding sites for cytochrome P450 3A4. Biochemistry. 2000; 39:5929–5939. [PubMed: 10821664]
12. Ueng YF, Kuwabara T, Chun YJ, Guengerich FP. Cooperativity in oxidations catalyzed by cytochrome P450 3A4. Biochemistry. 1997; 36:370–381. [PubMed: 9003190]
13. Roberts AG, Atkins WM. Energetics of heterotropic cooperativity between α-naphthoflavone and testosterone binding to CYP3A4. Arch Biochem Biophys. 2007; 463:89–101. [PubMed: 17459328]
14. Lampe JN, Fernandez C, Nath A, Atkins WM. Nile Red is a fluorescent allosteric substrate of cytochrome P450 3A4. Biochemistry. 2008; 47:509–516. [PubMed: 18092806]
15. Cameron MD, Wen B, Roberts AG, Atkins WM, Campbell AP, Nelson SD. Cooperative binding of acetaminophen and caffeine within the P450 3A4 active site. Chem Res Toxicol. 2007; 20:1434–1441. [PubMed: 17894464]
16. Maekawa K, Yoshimura T, Saito Y, Fujimura Y, Aohara F, Emoto C, Iwasaki K, Hanioka N, Narimatsu S, Niwa T, Sawada J. Functional characterization of CYP3A4. 16: catalytic activities toward midazolam and carbamazepine. Xenobiotica. 2009; 39:140–147. [PubMed: 19255940]
17. Domanski TL, He YA, Khan KK, Roussel F, Wang Q, Halpert JR. Phenylalanine and tryptophan scanning mutagenesis of CYP3A4 substrate recognition site residues and effect on substrate oxidation and cooperativity. Biochemistry. 2001; 40:10150–10160. [PubMed: 11513592]

Author Manuscript Author Manuscript Author Manuscript Author Manuscript

18. Frank DJ, Denisov IG, Sligar SG. Mixing apples and oranges: analysis of heterotropic cooperativity in cytochrome P450 3A4. Arch Biochem Biophys. 2009; 488:146–152. [PubMed: 19560436]
19. Denisov IG, Baas BJ, Grinkova YV, Sligar SG. Cooperativity in cytochrome P450 3A4: linkages in substrate binding, spin state, uncoupling, and product formation. J Biol Chem. 2007; 282:7066–7076. [PubMed: 17213193]
20. Frank DJ, Denisov IG, Sligar SG. Analysis of heterotropic cooperativity in cytochrome P450 3A4 using α-naphthoflavone and testosterone. J Biol Chem. 2011; 286:5540–5545. [PubMed: 21177853]
21. Roberts AG, Campbell AP, Atkins WM. The thermodynamic landscape of testosterone binding to cytochrome P450 3A4: ligand binding and spin state equilibria. Biochemistry. 2005; 44:1353–1366. [PubMed: 15667229]
22. Fernando H, Halpert JR, Davydov DR. Resolution of multiple substrate binding sites in cytochrome P450 3A4: the stoichiometry of the enzyme-substrate complexes probed by FRET and Job's titration. Biochemistry. 2006; 45:4199–4209. [PubMed: 16566594]
23. Fernando H, Davydov DR, Chin CC, Halpert JR. Role of subunit interactions in P450 oligomers in the loss of homotropic cooperativity in the cytochrome P450 3A4 mutant L211F/D214E/F304W. Arch Biochem Biophys. 2007; 460:129–140. [PubMed: 17274942]
24. Fernando H, Rumfeldt JA, Davydova NY, Halpert JR, Davydov DR. Multiple substrate-binding sites are retained in cytochrome P450 3A4 mutants with decreased cooperativity. Xenobiotica. 2011; 41:281–289. [PubMed: 21143007]
25. Renaud JP, Davydov DR, Heirwegh KP, Mansuy D, Hui Bon Hoa GH. Thermodynamic studies of substrate binding and spin transitions in human cytochrome P-450 3A4 expressed in yeast microsomes. Biochem J. 1996; 319(Pt 3):675–681. [PubMed: 8920966]
26. Isin EM, Guengerich FP. Kinetics and thermodynamics of ligand binding by cytochrome P450 3A4. J Biol Chem. 2006; 281:9127–9136. [PubMed: 16467307]
27. Isin EM, Guengerich FP. Multiple sequential steps involved in the binding of inhibitors to cytochrome P450 3A4. J Biol Chem. 2007; 282:6863–6874. [PubMed: 17200113]
28. Sevrioukova IF, Poulos TL. Structure and mechanism of the complex between cytochrome P4503A4 and ritonavir. Proc Natl Acad Sci U S A. 2010; 107:18422–18427. [PubMed: 20937904]
29. Sevrioukova IF, Poulos TL. Structural and mechanistic insights into the interaction of cytochrome P4503A4 with bromoergocryptine, a type I ligand. J Biol Chem. 2012; 287:3510–3517. [PubMed: 22157006]
30. Sevrioukova IF, Poulos TL. Interaction of human cytochrome P4503A4 with ritonavir analogs. Arch Biochem Biophys. 2012; 520:108–116. [PubMed: 22410611]
31. Sevrioukova IF, Poulos TL. Pyridine-substituted desoxyritonavir is a more potent cytochrome P450 3A4 inhibitor than ritonavir. J Med Chem. 2013; 56:3733–3741. [PubMed: 23586711]
32. Yamazaki H, Ueng YF, Shimada T, Guengerich FP. Roles of divalent metal ions in oxidations catalyzed by recombinant cytochrome P450 3A4 and replacement of NADPH-cytochrome P450 reductase with other flavoproteins, ferredoxin, and oxygen surrogates. Biochemistry. 1995; 34:8380–8389. [PubMed: 7599128]
33. Guengerich FP, Johnson WW. Kinetics of ferric cytochrome P450 reduction by NADPH-cytochrome P450 reductase: rapid reduction in the absence of substrate and variations among cytochrome P450 systems. Biochemistry. 1997; 36:14741–14750. [PubMed: 9398194]
34. Davydov DR, Fernando H, Baas BJ, Sligar SG, Halpert JR. Kinetics of dithionite-dependent reduction of cytochrome P450 3A4: heterogeneity of the enzyme caused by its oligomerization. Biochemistry. 2005; 44:13902–13913. [PubMed: 16229479]
35. Fernando H, Halpert JR, Davydov DR. Kinetics of electron transfer in the complex of cytochrome P450 3A4 with the flavin domain of cytochrome P450BM-3 as evidence of functional heterogeneity of the heme protein. Arch Biochem Biophys. 2008; 471:20–31. [PubMed: 18086551]
36. Davydov DR, Sineva EV, Sistla S, Davydova NY, Frank DJ, Sligar SG, Halpert JR. Electron transfer in the complex of membrane-bound human cytochrome P450 3A4 with the flavin domain

Author Manuscript Author Manuscript Author Manuscript Author Manuscript

of P450BM-3: the effect of oligomerization of the heme protein and intermittent modulation of the spin equilibrium. Biochim Biophys Acta. 2010; 1797:378–390. [PubMed: 20026040]

37. Koley AP, Buters JT, Robinson RC, Markowitz A, Friedman FK. CO binding kinetics of human cytochrome P450 3A4. Specific interaction of substrates with kinetically distinguishable conformers. J Biol Chem. 1995; 270:5014–5018. [PubMed: 7890608]
38. Koley AP, Robinson RC, Friedman FK. Cytochrome P450 conformation and substrate interactions as probed by CO binding kinetics. Biochimie. 1996; 78:706–713. [PubMed: 9010599]
39. Koley AP, Buters JT, Robinson RC, Markowitz A, Friedman FK. Differential mechanisms of cytochrome P450 inhibition and activation by α-naphthoflavone. J Biol Chem. 1997; 272:3149–3152. [PubMed: 9013547]
40. Kumar S, Davydov DR, Halpert JR. Role of cytochrome b_5 in modulating peroxide-supported CYP3A4 activity: evidence for a conformational transition and cytochrome P450 heterogeneity. Drug Metab Dispos. 2005; 33:1131–1136. [PubMed: 15870379]
41. Davydov DR, Halpert JR, Renaud JP, Hui Bon Hoa G. Conformational heterogeneity of cytochrome P450 3A4 revealed by high pressure spec-troscopy. Biochem Biophys Res Commun. 2003; 312:121–130. [PubMed: 14630029]
42. Davydov DR, Baas BJ, Sligar SG, Halpert JR. Allosteric mechanisms in cytochrome P450 3A4 studied by high-pressure spectroscopy: pivotal role of substrate-induced changes in the accessibility and degree of hydration of the heme pocket. Biochemistry. 2007; 46:7852–7864. [PubMed: 17555301]
43. Kapelyukh Y, Paine MJ, Marechal JD, Sutcliffe MJ, Wolf CR, Roberts GC. Multiple substrate binding by cytochrome P450 3A4: estimation of the number of bound substrate molecules. Drug Metab Dispos. 2008; 36:2136–2144. [PubMed: 18645035]
44. Dabrowski MJ, Schrag ML, Wienkers LC, Atkins WM. Pyrene-pyrene complexes at the active site of cytochrome P450 3A4: evidence for a multiple substrate binding site. J Am Chem Soc. 2002; 124:11866–11867. [PubMed: 12358527]
45. Nath A, Fernandez C, Lampe JN, Atkins WM. Spectral resolution of a second binding site for Nile Red on cytochrome P4503A4. Arch Biochem Biophys. 2008; 474:198–204. [PubMed: 18395506]
46. Davydov DR, Davydova NY, Sineva EV, Kufareva I, Halpert JR. Pivotal role of P450-P450 interactions in CYP3A4 allostery: the case of α-naphthoflavone. Biochem J. 2013; 453:219–230. [PubMed: 23651100]
47. Nath A, Koo PK, Rhoades E, Atkins WM. Allosteric effects on substrate dissociation from cytochrome P450 3A4 in nanodiscs observed by ensemble and single-molecule fluorescence spectroscopy. J Am Chem Soc. 2008; 130:15746–15747. [PubMed: 18980315]
48. Stresser DM, Blanchard AP, Turner SD, Erve JC, Dandeneau AA, Miller VP, Crespi CL. Substrate-dependent modulation of CYP3A4 catalytic activity: analysis of 27 test compounds with four fluorometric substrates. Drug Metab Dispos. 2000; 28:1440–1448. [PubMed: 11095581]
49. Chougnet A, Grinkova Y, Ricard D, Sligar S, Woggon WD. Fluorescent probes for rapid screening of potential drug-drug interactions at the CYP3A4 level. ChemMedChem. 2007; 2:717–724. [PubMed: 17357170]
50. Lampe JN, Atkins WM. Time-resolved fluorescence studies of heterotropic ligand binding to cytochrome P450 3A4. Biochemistry. 2006; 45:12204–12215. [PubMed: 17014074]
51. Tsalkova TN, Davydova NY, Halpert JR, Davydov DR. Mechanism of interactions of α-naphthoflavone with cytochrome P450 3A4 explored with an engineered enzyme bearing a fluorescent probe. Biochemistry. 2007; 46:106–119. [PubMed: 17198380]
52. Davydov DR, Davydova NY, Tsalkova TN, Halpert JR. Effect of glutathione on homo- and heterotropic cooperativity in cytochrome P450 3A4. Arch Biochem Biophys. 2008; 471:134–145. [PubMed: 18206979]
53. Gartner CA, Wen B, Wan J, Becker RS, Jones G 2nd, Gygi SP, Nelson SD. Photochromic agents as tools for protein structure study: lapachenole is a photoaffinity ligand of cytochrome P450 3A4. Biochemistry. 2005; 44:1846–1855. [PubMed: 15697210]
54. Wen B, Doneanu CE, Gartner CA, Roberts AG, Atkins WM, Nelson SD. Fluorescent photoaffinity labeling of cytochrome P450 3A4 by lapachenole: identification of modification sites by mass spectrometry. Biochemistry. 2005; 44:1833–1845. [PubMed: 15697209]

Author Manuscript Author Manuscript Author Manuscript Author Manuscript

55. Kim JS, Ahn T, Yim SK, Yun CH. Differential effect of copper (II) on the cytochrome P450 enzymes and NADPH-cytochrome P450 reductase: inhibition of cytochrome P450-catalyzed reactions by copper (II) ion. Biochemistry. 2002; 41:9438–9447. [PubMed: 12135366]
56. Kim JS, Yun CH. Inhibition of human cytochrome P450 3A4 activity by zinc(II) ion. Toxicol Lett. 2005; 156:341–350. [PubMed: 15763633]
57. Baylon JL, Lenov IL, Sligar SG, Tajkhorshid E. Characterizing the membrane-bound state of cytochrome P450 3A4: structure, depth of insertion, and orientation. J Am Chem Soc. 2013; 135:8542–8851. [PubMed: 23697766]
58. Pearson JT, Hill JJ, Swank J, Isoherranen N, Kunze KL, Atkins WM. Surface plasmon resonance analysis of antifungal azoles binding to CYP3A4 with kinetic resolution of multiple binding orientations. Biochemistry. 2006; 45:6341–6353. [PubMed: 16700545]
59. Pearson J, Dahal UP, Rock D, Peng CC, Schenk JO, Joswig-Jones C, Jones JP. The kinetic mechanism for cytochrome P450 metabolism of type II binding compounds: evidence supporting direct reduction. Arch Biochem Biophys. 2011; 511:69–79. [PubMed: 21530484]
60. Das A, Zhao J, Schatz GC, Sligar SG, Van Duyne RP. Screening of type I and II drug binding to human cytochrome P450-3A4 in nanodiscs by localized surface plasmon resonance spectroscopy. Anal Chem. 2009; 81:3754–3759. [PubMed: 19364136]
61. Cameron MD, Wen B, Allen KE, Roberts AG, Schuman JT, Campbell AP, Kunze KL, Nelson SD. Cooperative binding of midazolam with testosterone and α-naphthoflavone within the CYP3A4 active site: a NMR T1 paramagnetic relaxation study. Biochemistry. 2005; 44:14143–14151. [PubMed: 16245930]
62. Roberts AG, Yang J, Halpert JR, Nelson SD, Thummel KT, Atkins WM. The structural basis for homotropic and heterotropic cooperativity of midazolam metabolism by human cytochrome P450 3A4. Biochemistry. 2011; 50:10804–10818. [PubMed: 21992114]
63. Kijac AZ, Li Y, Sligar SG, Rienstra CM. Magic-angle spinning solid-state NMR spectroscopy of nanodisc-embedded human CYP3A4. Biochemistry. 2007; 46:13696–13703. [PubMed: 17985934]
64. Conner KP, Vennam P, Woods CM, Krzyaniak MD, Bowman MK, Atkins WM. 1,2,3-Triazoleheme interactions in cytochrome P450: functionally competent triazole-water-heme complexes. Biochemistry. 2012; 51:6441–6457. [PubMed: 22809252]
65. Mak PJ, Denisov IG, Grinkova YV, Sligar SG, Kincaid JR. Defining CYP3A4 structural responses to substrate binding. Raman spectroscopic studies of a nanodisc-incorporated mammalian cytochrome P450. J Am Chem Soc. 2011; 133:1357–1366. [PubMed: 21207936]
66. Obach RS. Mechanism of cytochrome P4503A4- and 2D6-catalyzed dehydrogenation of ezlopitant as probed with isotope effects using five deuterated analogs. Drug Metab Dispos. 2001; 29:1599–1607. [PubMed: 11717179]
67. Krauser JA, Guengerich FP. Cytochrome P450 3A4-catalyzed testosterone 6β-hydroxylation stereochemistry, kinetic deuterium isotope effects, and rate-limiting steps. J Biol Chem. 2005; 280:19496–19506. [PubMed: 15772082]
68. Woods CM, Fernandez C, Kunze KL, Atkins WM. Allosteric activation of cytochrome P450 3A4 by α-naphthoflavone: branch point regulation revealed by isotope dilution analysis. Biochemistry. 2011; 50:10041–10051. [PubMed: 22004098]
69. Joseph S, Rusling JF, Lvov YM, Friedberg T, Fuhr U. An amperometric biosensor with human CYP3A4 as a novel drug screening tool. Biochem Pharmacol. 2003; 65:1817–1826. [PubMed: 12781333]
70. Xue Q, Kato D, Kamata T, Guo Q, You T, Niwa O. Human cytochrome P450 3A4 and a carbon nanofiber modified film electrode as a platform for the simple evaluation of drug metabolism and inhibition reactions. Analyst. 2013; 138:6463–6468. [PubMed: 24027778]
71. Sadeghi SJ, Ferrero S, Di Nardo G, Gilardi G. Drug-drug interactions and cooperative effects detected in electrochemically driven human cytochrome P450 3A4. Bioelectrochemistry. 2012; 86:87–91. [PubMed: 22480862]
72. Hendricks NR, Waryo TT, Arotiba O, Jahed N, Baker PGL, Iwuoha EI. Microsomal cytochrome P450-3A4 (CYP3A4) nanobiosensor for the determination of 2,4-dichlorophenol - an endocrine disruptor compound. Electrochim Acta. 2009; 54:1925–1931.

Author Manuscript Author Manuscript Author Manuscript Author Manuscript

73. Ignaszak A, Hendricks N, Waryo T, Songa E, Jahed N, Ngece R, Al-Ahmed A, Kgarebe B, Baker P, Iwuoha EI. Novel therapeutic biosensor for indinavir - a protease inhibitor antiretroviral drug. J Pharm Biomed Anal. 2009; 49:498–501. [PubMed: 19056199]
74. Mie Y, Suzuki M, Komatsu Y. Electrochemically driven drug metabolism by membranes containing human cytochrome P450. J Am Chem Soc. 2009; 131:6646–6647. [PubMed: 19402636]
75. Larsen AT, May EM, Auclair K. Predictable stereoselective and chemoselective hydroxylations and epoxidations with P450 3A4. J Am Chem Soc. 2011; 133:7853–7858. [PubMed: 21528858]
76. Johnson EF, Stout CD. Structural diversity of human xenobiotic-metabolizing cytochrome P450 monooxygenases. Biochem Biophys Res Commun. 2005; 338:331–336. [PubMed: 16157296]
77. Williams PA, Cosme J, Vinkovic DM, Ward A, Angove HC, Day PJ, Vonrhein C, Tickle IJ, Jhoti H. Crystal structures of human cytochrome P450 3A4 bound to metyrapone and progesterone. Science. 2004; 305:683–686. [PubMed: 15256616]
78. Yano JK, Wester MR, Schoch GA, Griffin KJ, Stout CD, Johnson EF. The structure of human microsomal cytochrome P450 3A4 determined by X-ray crystallography to 2.05-Å resolution. J Biol Chem. 2004; 279:38091–38094. [PubMed: 15258162]
79. Ekroos M, Sjogren T. Structural basis for ligand promiscuity in cytochrome P450 3A4. Proc Natl Acad Sci U S A. 2006; 103:13682–13687. [PubMed: 16954191]
80. Sevrioukova IF, Poulos TL. Dissecting cytochrome P450 3A4-ligand interactions using ritonavir analogues. Biochemistry. 2013; 52:4474–4481. [PubMed: 23746300]
81. Sevrioukova IF, Poulos TL. Ritonavir analogues as a probe for deciphering the cytochrome P450 3A4 inhibitory mechanism. Curr Topics Med Chem. 2014; 14:1348–1355.
82. Cupp-Vickery J, Anderson R, Hatziris Z. Crystal structures of ligand complexes of P450eryF exhibiting homotropic cooperativity. Proc Natl Acad Sci U S A. 2000; 97:3050–3055. [PubMed: 10716705]
83. Park H, Lee S, Suh J. Structural and dynamical basis of broad substrate specificity, catalytic mechanism, and inhibition of cytochrome P450 3A4. J Am Chem Soc. 2005; 127:13634–13642. [PubMed: 16190729]
84. Fishelovitch D, Hazan C, Shaik S, Wolfson HJ, Nussinov R. Structural dynamics of the cooperative binding of organic molecules in the human cytochrome P450 3A4. J Am Chem Soc. 2007; 129:1602–1611. [PubMed: 17284003]
85. Sun H, Moore C, Dansette PM, Kumar S, Halpert JR, Yost GS. Dehydrogenation of the indoline-containing drug 4-chloro-N-(2-methyl-1-indolinyl)-3-sulfamoylbenzamide (indapamide) by CYP3A4: correlation with in silico predictions. Drug Metab Dispos. 2009; 37:672–684. [PubMed: 19074530]
86. Sun H, Scott DO. Metabolism of 4-aminopiperidine drugs by cytochrome P450s: molecular and quantum mechanical insights into drug design. ACS Med Chem Lett. 2011; 2:638–643. [PubMed: 21841964]
87. Li W, Liu H, Luo X, Zhu W, Tang Y, Halpert JR, Jiang H. Possible pathway(s) of metyrapone egress from the active site of cytochrome P450 3A4: a molecular dynamics simulation. Drug Metab Dispos. 2007; 35:689–696. [PubMed: 17251305]
88. Fishelovitch D, Shaik S, Wolfson HJ, Nussinov R. Theoretical characterization of substrate access/exit channels in the human cytochrome P450 3A4 enzyme: involvement of phenylalanine residues in the gating mechanism. J Phys Chem. 2009; 113:13018–13025.
89. Krishnamoorthy N, Gajendrarao P, Thangapandian S, Lee Y, Lee KW. Probing possible egress channels for multiple ligands in human CYP3A4: a molecular modeling study. J Mol Model. 2009; 16:607–614. [PubMed: 19727863]
90. Shahrokh K, Cheatham TE 3rd, Yost GS. Conformational dynamics of CYP3A4 demonstrate the important role of Arg212 coupled with the opening of ingress, egress and solvent channels to dehydrogenation of 4-hydroxytamoxifen. Biochim Biophys Acta. 2012; 1820:1605–1617. [PubMed: 22677141]
91. Bren U, Oostenbrink C. Cytochrome P450 3A4 inhibition by ketoconazole: tackling the problem of ligand cooperativity using molecular dynamics simulations and free- energy calculations. J Chem Inf Model. 2012; 52:1573–1582. [PubMed: 22587011]

Author Manuscript Author Manuscript Author Manuscript Author Manuscript

92. Fishelovitch D, Shaik S, Wolfson HJ, Nussinov R. How does the reductase help to regulate the catalytic cycle of cytochrome P450 3A4 using the conserved water channel? J Phys Chem. 2010; 114:5964–5970.

93. Denisov IG, Shih AY, Sligar SG. Structural differences between soluble and membrane bound cytochrome P450s. J Inorg Biochem. 2012; 108:150–158. [PubMed: 22244217]

94. Berka K, Paloncyova M, Anzenbacher P, Otyepka M. Behavior of human cytochromes P450 on lipid membranes. J Phys Chem. 2013; 117:11556–11564.

95. Liu X, Wang X, Jiang H. A steered molecular dynamics method with direction optimization and its applications on ligand molecule dissociation. J Biochem Biophys Methods. 2008; 70:857–864. [PubMed: 18031823]

96. Yang K, Liu X, Wang X, Jiang H. A steered molecular dynamics method with adaptive direction adjustments. Biochem Biophys Res Commun. 2009; 379:494–498. [PubMed: 19118521]

97. Torimoto N, Ishii I, Hata M, Nakamura H, Imada H, Ariyoshi N, Ohmori S, Igarashi T, Kitada M. Direct interaction between substrates and endogenous steroids in the active site may change the activity of cytochrome P450 3A4. Biochemistry. 2003; 42:15068–15077. [PubMed: 14690416]

98. Fishelovitch D, Hazan C, Hirao H, Wolfson HJ, Nussinov R, Shaik S. QM/MM study of the active species of the human cytochrome P450 3A4, and the influence thereof of the multiple substrate binding. J Phys Chem. 2007; 111:13822–13832.

99. Zhang Y, Morisetti P, Kim J, Smith L, Lin H. Regioselectivity preference of testosterone hydroxylation by cytochrome P450 3A4. Theor Chem Acc. 2008; 121:313–319.

100. Kongsted J, Ryde U. An improved method to predict the entropy term with the MM/PBSA approach. J Comput Aided Mol Des. 2009; 23:63–71. [PubMed: 18781280]

101. Zhang Y, Lin H. Quantum tunneling in testosterone 6β-hydroxylation by cytochrome P450: reaction dynamics calculations employing multiconfiguration molecular-mechanical potential energy surfaces. J Phys Chem. 2009; 113:11501–11508.

102. Lee JY, Kang NS, Kang YK. Binding free energies of inhibitors to iron porphyrin complex as a model for cytochrome P450. Biopolymers. 2012; 97:219–228. [PubMed: 22113809]

103. de Groot MJ, Ekins S. Pharmacophore modeling of cytochromes P450. Adv Drug Deliv Rev. 2002; 54:367–383. [PubMed: 11922953]

104. Wang Y, Han KL, Sheng-Li Y, Yang L. Structural determinants of steroids for cytochrome P450 3A4-mediated metabolism. J Mol Struct. 2004; 710:215–221.

105. Ekins S, Bravi G, Wikel JH, Wrighton SA. Three-dimensional-quantitative structure activity relationship analysis of cytochrome P-450 3A4 substrates. J Pharmacol Exp Ther. 1999; 291:424–433. [PubMed: 10490933]

106. Ekins S, Bravi G, Binkley S, Gillespie JS, Ring BJ, Wikel JH, Wrighton SA. Three- and four-dimensional quantitative structure activity relationship analyses of cytochrome P-450 3A4 inhibitors. J Pharmacol Exp Ther. 1999; 290:429–438. [PubMed: 10381809]

107. Riley RJ, Parker AJ, Trigg S, Manners CN. Development of a generalized, quantitative physicochemical model of CYP3A4 inhibition for use in early drug discovery. Pharm Res. 2001; 18:652–655. [PubMed: 11465421]

108. Ekins S, Stresser DM, Williams JA. In vitro and pharmacophore insights into CYP3A enzymes. Trends Pharmacol Sci. 2003; 24:161–166. [PubMed: 12707001]

109. Ekins S, Berbaum J, Harrison RK. Generation and validation of rapid computational filters for CYP2D6 and CYP3A4. Drug Metab Dispos. 2003; 31:1077–1080. [PubMed: 12920160]

110. Regev-Shoshani G, Shoseyov O, Kerem Z. Influence of lipophilicity on the interactions of hydroxy stilbenes with cytochrome P450 3A4. Biochem Biophys Res Commun. 2004; 323:668–673. [PubMed: 15369802]

111. Singh SB, Shen LQ, Walker MJ, Sheridan RP. A model for predicting likely sites of CYP3A4-mediated metabolism on drug-like molecules. J Med Chem. 2003; 46:1330–1336. [PubMed: 12672233]

112. Mao B, Gozalbes R, Barbosa F, Migeon J, Merrick S, Kamm K, Wong E, Costales C, Shi W, Wu C, Froloff N. QSAR modeling of in vitro inhibition of cytochrome P450 3A4. J Chem Inf Model. 2006; 46:2125–2134. [PubMed: 16995743]

Author Manuscript Author Manuscript Author Manuscript Author Manuscript

113. Lill MA, Dobler M, Vedani A. Prediction of small-molecule binding to cytochrome P450 3A4: flexible docking combined with multidimensional QSAR. Chem Med Chem. 2006; 1:73–81. [PubMed: 16892339]

114. Sheridan RP, Korzekwa KR, Torres RA, Walker MJ. Empirical regioselectivity models for human cytochromes P450 3A4, 2D6, and 2C9. J Med Chem. 2007; 50:3173–3184. [PubMed: 17579382]

115. Kjellander B, Masimirembwa CM, Zamora I. Exploration of enzyme-ligand interactions in CYP2D6 and 3A4 homology models and crystal structures using a novel computational approach. J Chem Inf Model. 2007; 47:1234–1247. [PubMed: 17381082]

116. Jayakanthan M, Chandrasekar S, Muthukumaran J, Mathur PP. Analysis of CYP3A4-HIV-1 protease drugs interactions by computational methods for highly active antiretroviral therapy in HIV/AIDS. J Mol Graph Model. 2010; 28:455–463. [PubMed: 19931478]

117. Dapkunas J, Sazonovas A, Japertas P. Probabilistic prediction of the human CYP3A4 and CYP2D6 metabolism sites. Chem Biodivers. 2009; 6:2101–2106. [PubMed: 19937844]

118. Didziapetris R, Dapkunas J, Sazonovas A, Japertas P. Trainable structure-activity relationship model for virtual screening of CYP3A4 inhibition. J Comput Aided Mol Des. 2010; 24:891–906. [PubMed: 20814717]

119. Handa K, Nakagome I, Yamaotsu N, Gouda H, Hirono S. Three-dimensional quantitative structure-activity relationship analysis of inhibitors of human and rat cytochrome P4503A enzymes. Drug Metab Pharmacokinet. 2013; 28:345–355. [PubMed: 23358262]

120. Tie Y, McPhail B, Hong H, Pearce BA, Schnackenberg LK, Ge W, Buzatu DA, Wilkes JG, Fuscoe JC, Tong W, Fowler BA, Beger RD, Demchuk E. Modeling chemical interaction profiles: II. Molecular docking, spectral data-activity relationship, and structure-activity relationship models for potent and weak inhibitors of cytochrome P450 CYP3A4 isozyme. Molecules. 2013; 17:3407–3460. [PubMed: 22421793]

121. Jensen BF, Vind C, Padkjaer SB, Brockhoff PB, Refsgaard HH. In silico prediction of cytochrome P450 2D6 and 3A4 inhibition using Gaussian kernel weighted *k*-nearest neighbor and extended connectivity fingerprints, including structural fragment analysis of inhibitors versus noninhibitors. J Med Chem. 2007; 50:501–511. [PubMed: 17266202]

122. Zhou D, Afzelius L, Grimm SW, Andersson TB, Zauhar RJ, Zamora I. Comparison of methods for the prediction of the metabolic sites for CYP3A4-mediated metabolic reactions. Drug Metab Dispos. 2006; 34:976–983. [PubMed: 16540587]

123. Vedani A, Dobler M, Lill MA. The challenge of predicting drug toxicity *in silico* . Basic Clin Pharmacol Toxicol. 2006; 99:195–208. [PubMed: 16930291]

124. Sun H, Scott DO. Structure-based drug metabolism predictions for drug design. Chem Biol Drug Des. 2010; 75:3–17. [PubMed: 19878193]

Author Manuscript Author Manuscript Author Manuscript Author Manuscript

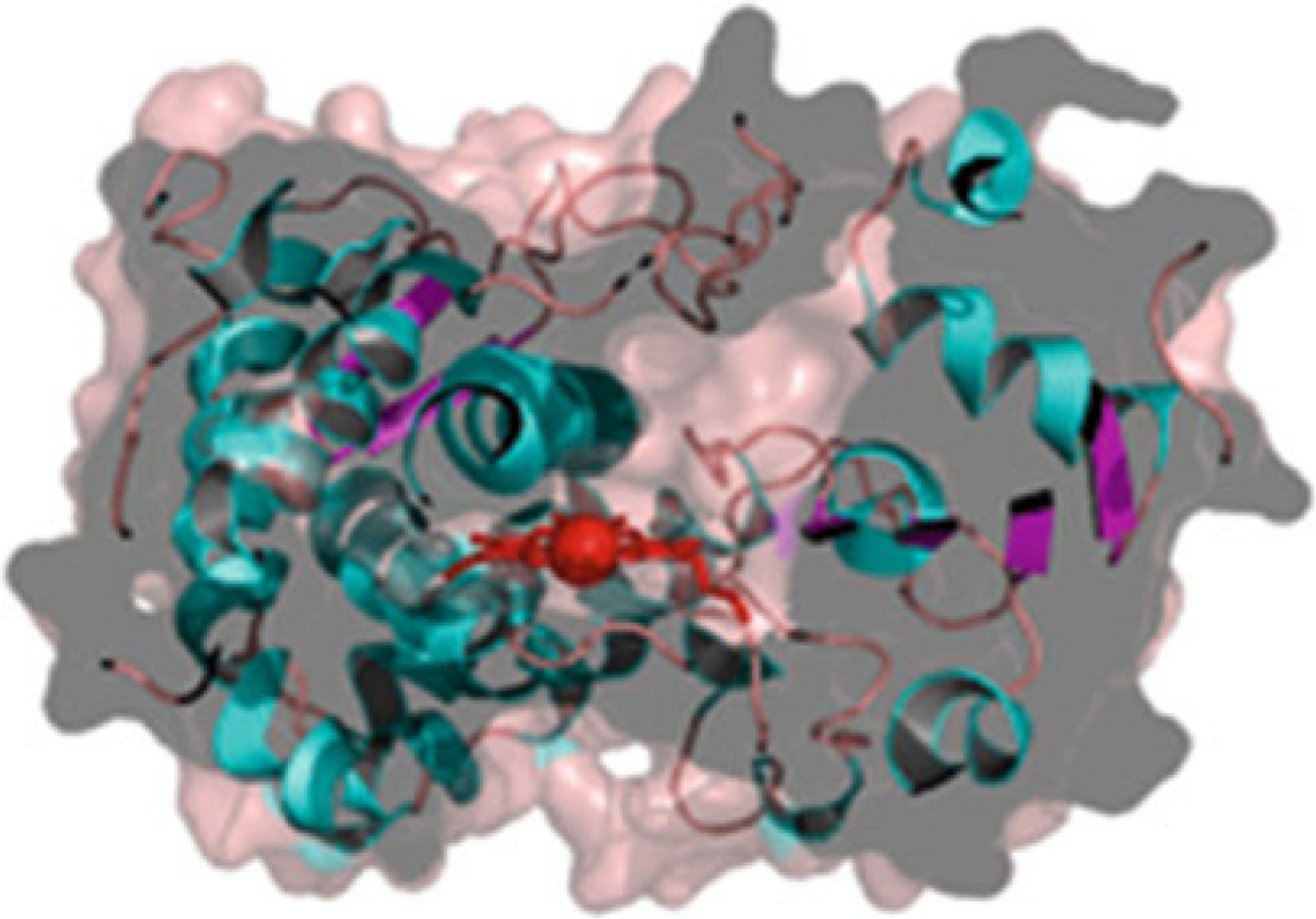

Fig. 3.1.

Crystal structure of ligand-free CYP3A4 (Protein Data Base ID 1TQN). A cross-section of solvent-accessible surface is shown to display the active-site cavity. Helices, strands and loops are in *cyan*, *magenta* and *beige*, respectively, and the heme is *red*

Author Manuscript Author Manuscript Author Manuscript Author Manuscript

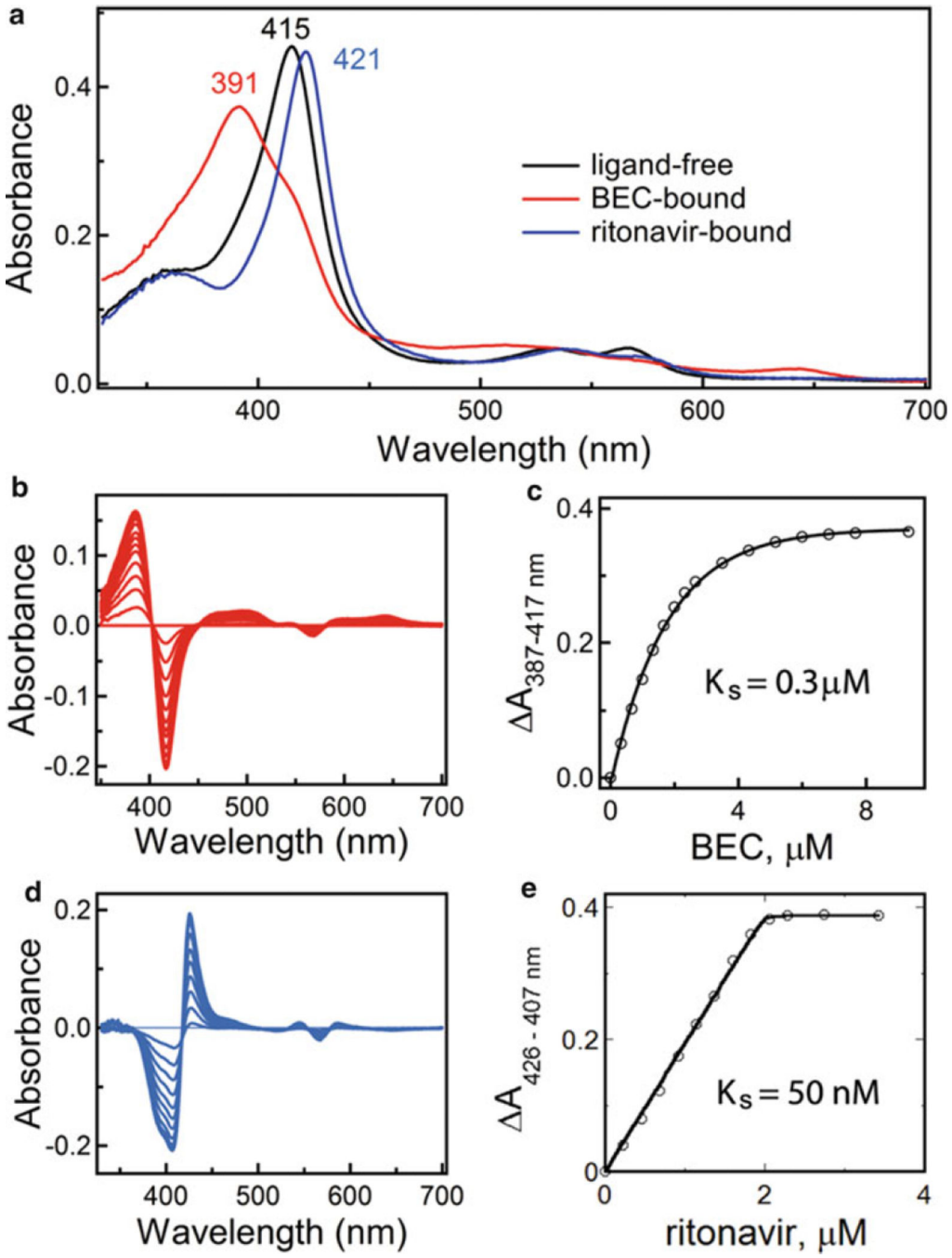

Fig. 3.2.

Spectral changes induced by BEC and ritonavir in CYP3A4. (**a**) Upon binding, BEC causes a *blue* shift in the Soret band, whereas ritonavir induces a *red* shift (type I and type II spectral changes, respectively). (**b, c**) Difference absorbance spectra recorded during BEC binding and a plot of absorbance changes vs. ligand concentration, respectively. (**d, e**) Difference absorbance spectra recorded during ritonavir binding and a plot of absorbance changes vs. ligand concentration, respectively. Spectral dissociation constants (K_s) calculated from titration plots are indicated

Author Manuscript Author Manuscript Author Manuscript Author Manuscript

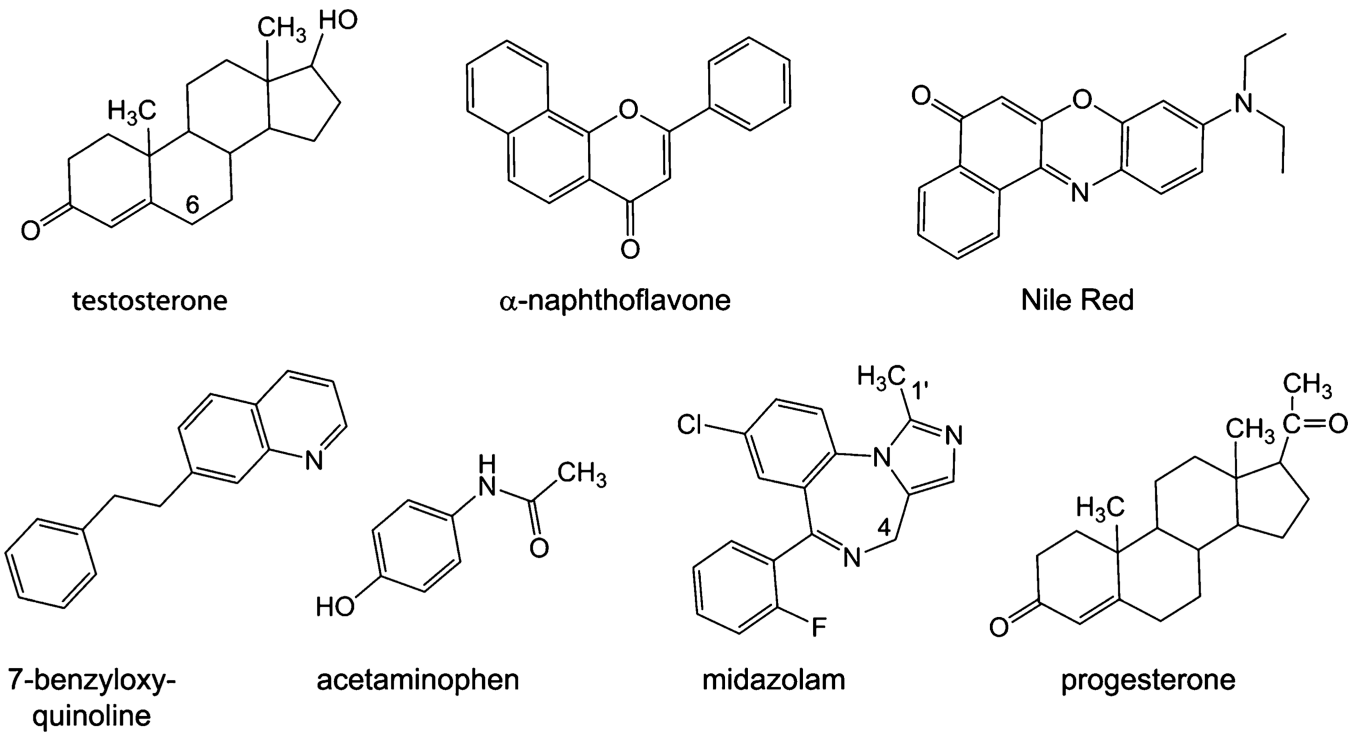

Fig. 3.3.

CYP3A4 substrates that display binding cooperativity. Sites of metabolism in testosterone (C6) and midazolam (C4 and C1′) are indicated

Author Manuscript Author Manuscript Author Manuscript Author Manuscript

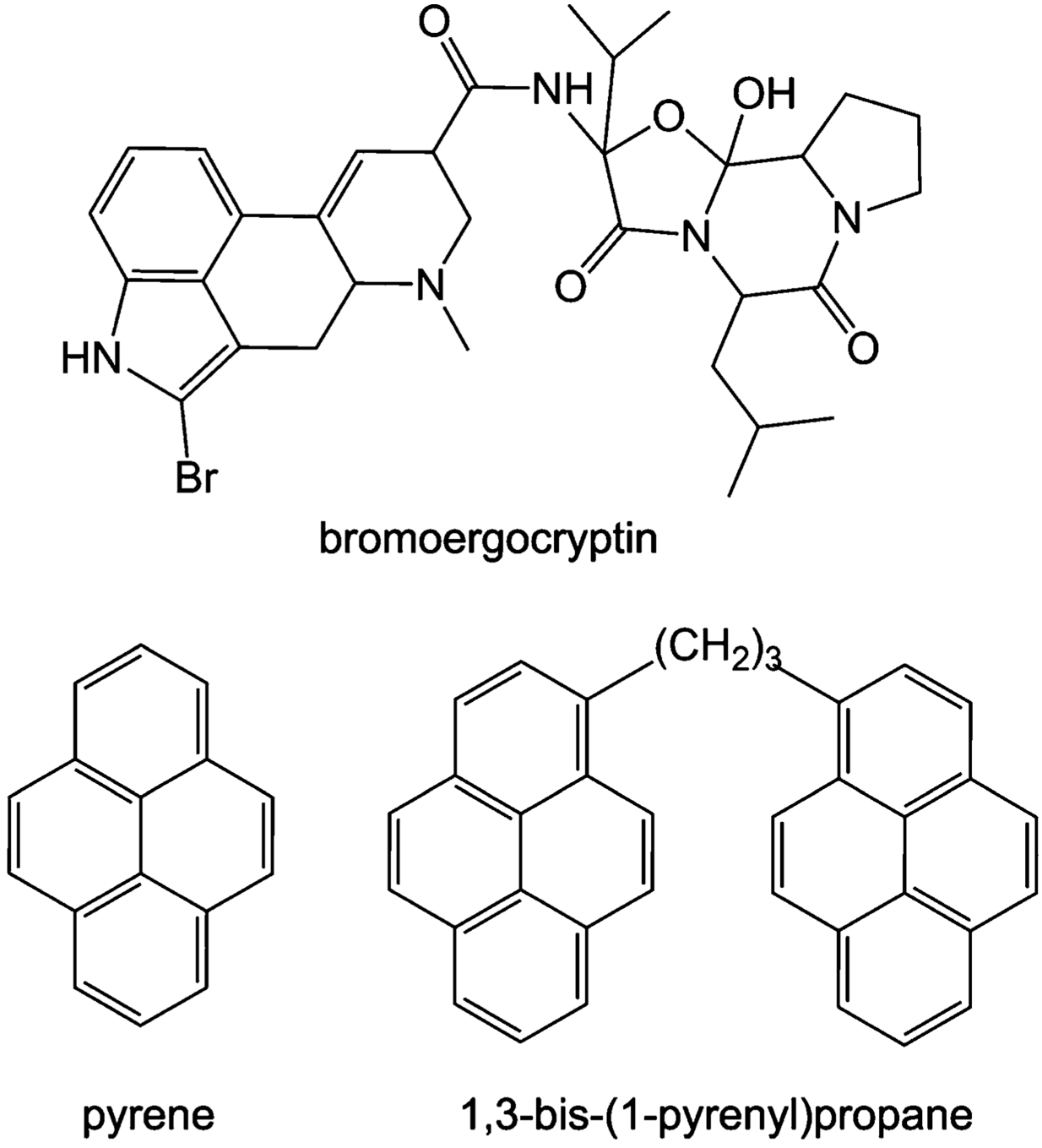

Fig. 3.4.
Fluorescent substrates of CYP3A4

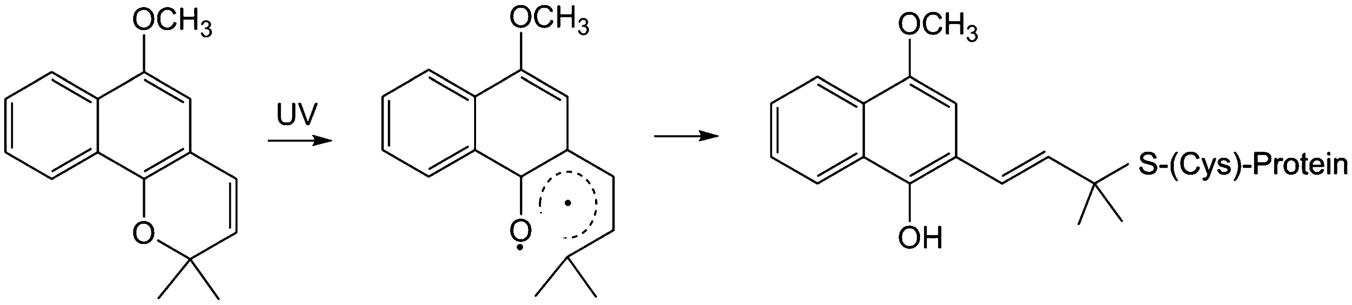

Fig. 3.5.
CYP3A4 labeling by photoactivated lapachenole [54]

Author Manuscript Author Manuscript Author Manuscript Author Manuscript

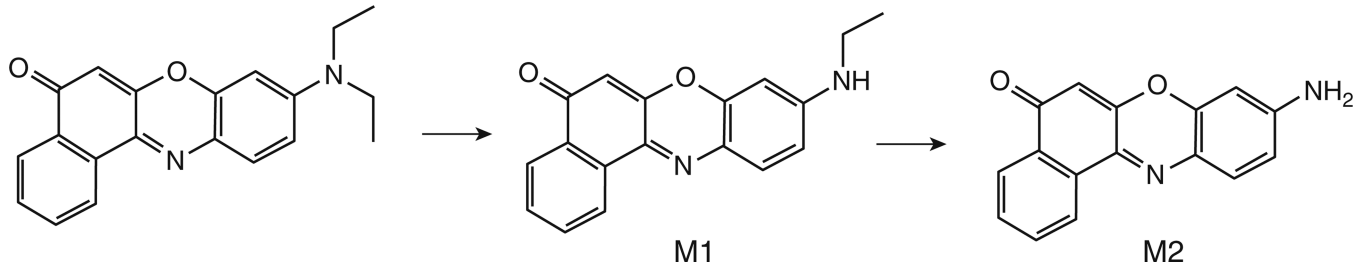

Fig. 3.6.
Sequential demethylation of Nile Red catalyzed by CYP3A4 [68]

Author Manuscript Author Manuscript Author Manuscript Author Manuscript

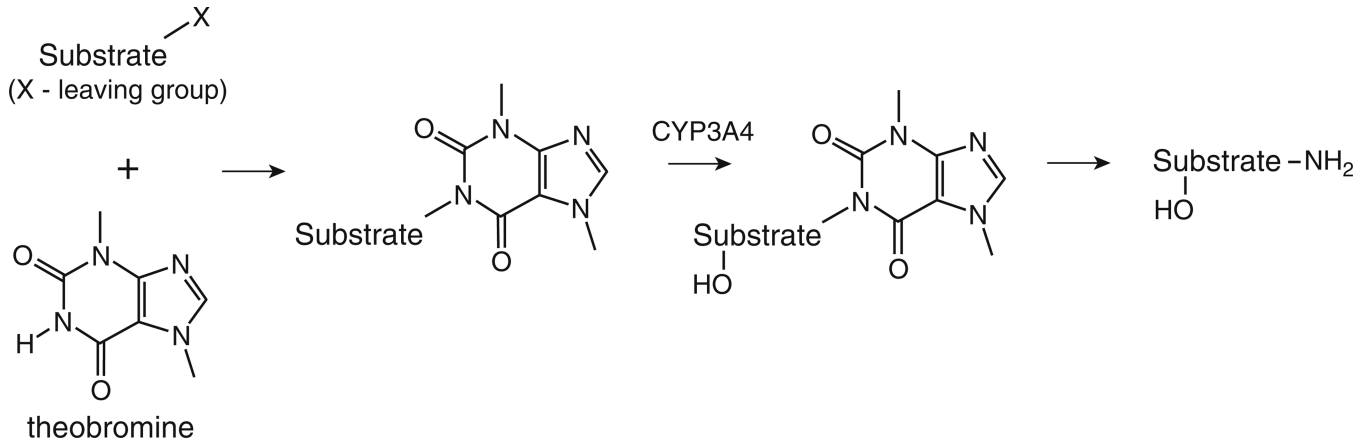

Fig. 3.7.
Theobromine auxiliary for controllable oxidations by CYP3A4 [75]

Author Manuscript Author Manuscript Author Manuscript Author Manuscript

Author Manuscript Author Manuscript Author Manuscript Author Manuscript

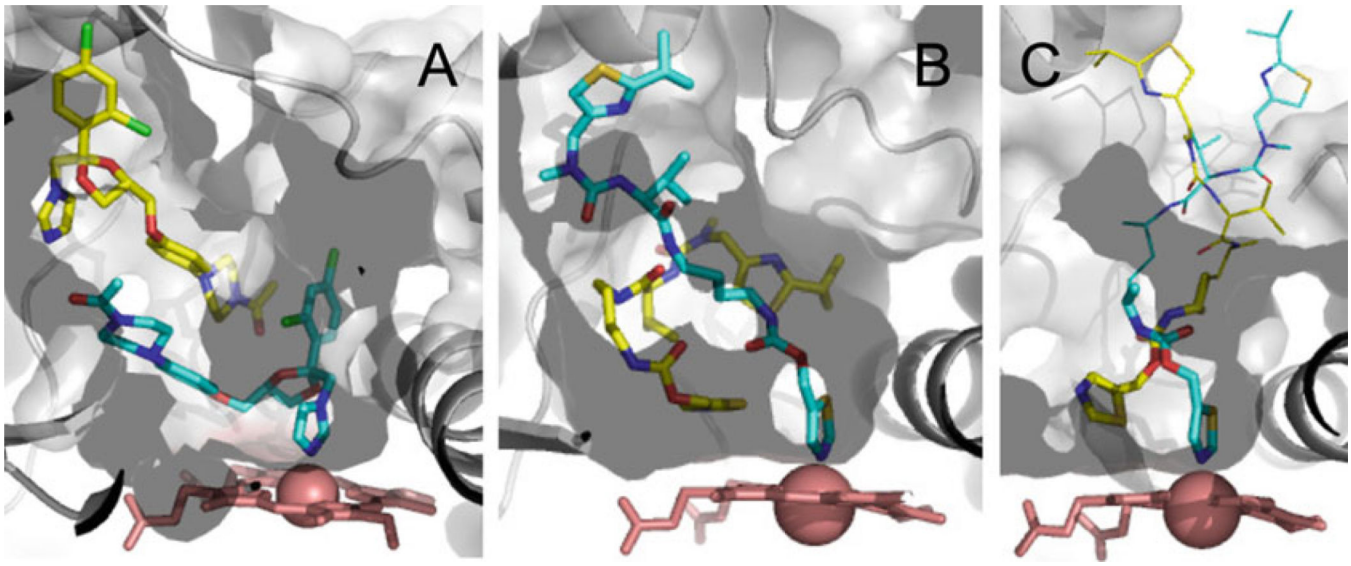

Fig. 3.8.

Crystal structures of CYP3A4 with two inhibitors bound in the active site. (**a**) Ketoconazole molecules bind in a parallel tandem fashion (2VOM structure) [79]. (**b, c**) Ritonavir analogs GS4 and GS5 associate in a perpendicular and intertwined parallel mode, respectively (PDB ID 4K9T and 4K9U) [80]. Disordered parts of GS5 that are not seen in the X-ray structure are shown as *thin lines*. Heme is in *pink* and the heme-bound ligands are in *cyan*

Author Manuscript Author Manuscript Author Manuscript Author Manuscript

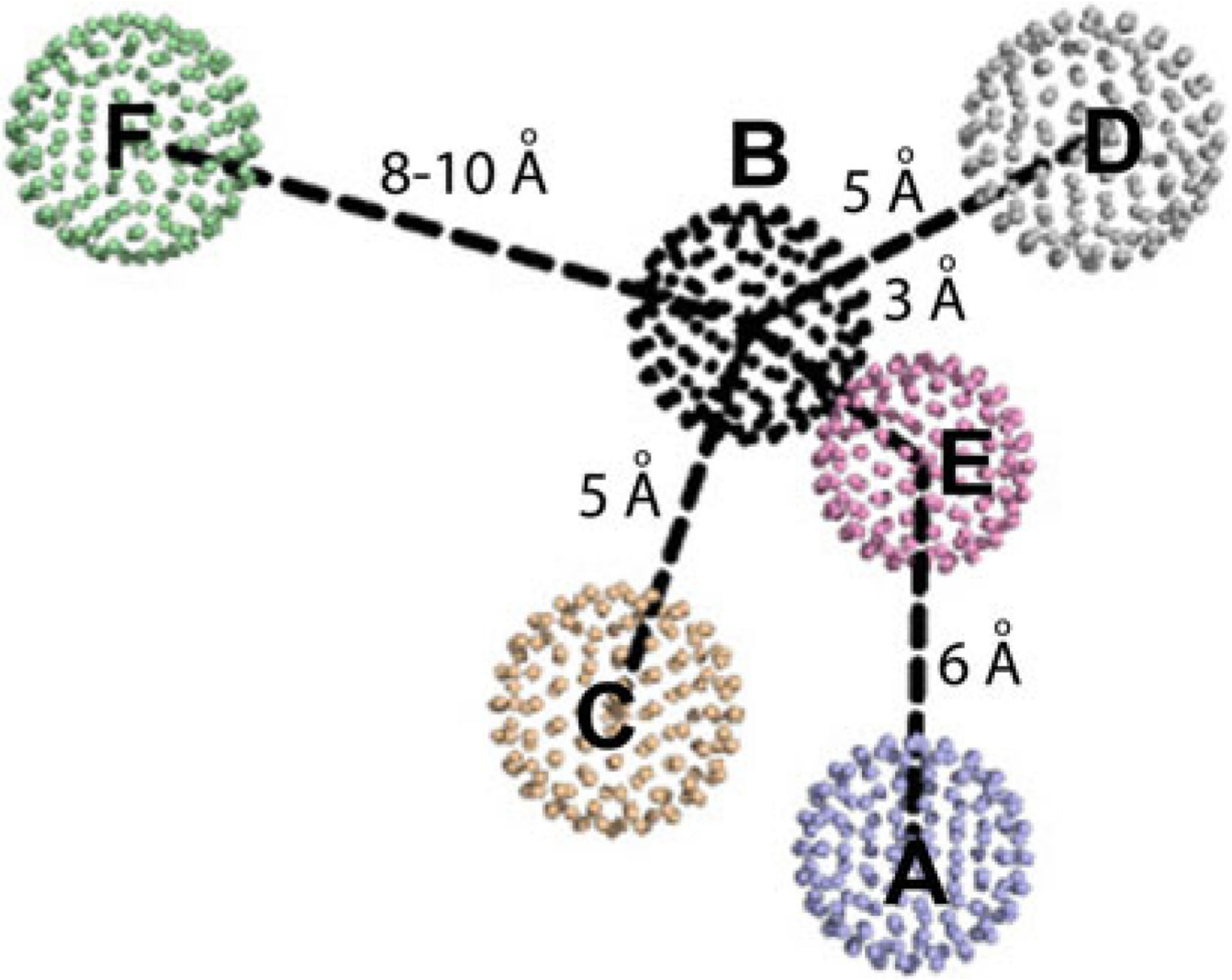

Fig. 3.9.

Pharmacophore for a potent CYP3A4 inhibitor. Pharmacophoric features were derived based on studies with ritonavir analogs [28, 30, 31, 80] and include: (**a**) strong heme-ligating nitrogen donor; (**b**) flexible backbone; (**c**) aromatic group; (**d**) hydrophobic group; (**e**) hydrogen donor/acceptor, and (**f**) polyfunctional end-group

Author Manuscript Author Manuscript Author Manuscript Author Manuscript

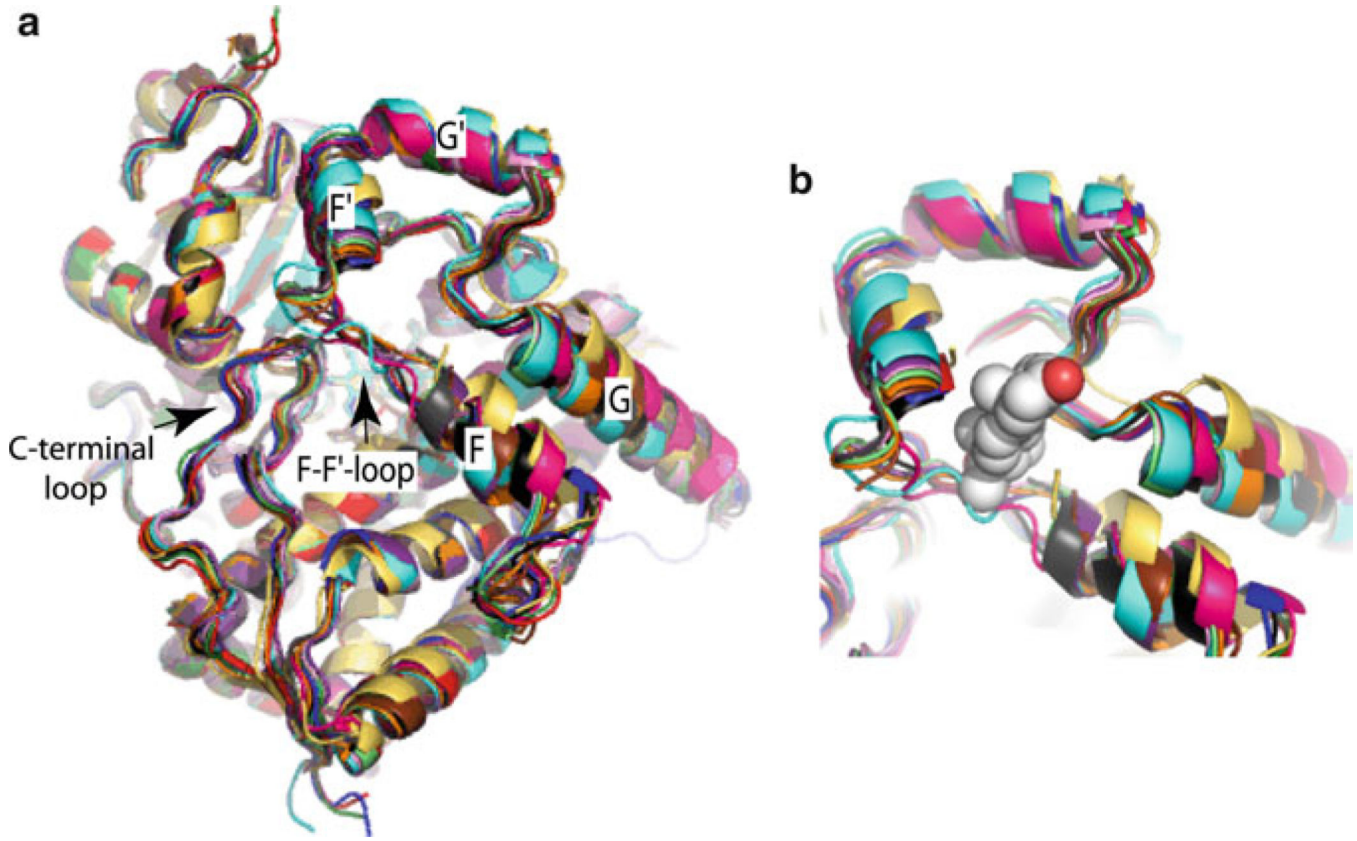

Fig. 3.10.

Superposition of all available structures of CYP3A4. (**a**) A general view showing that ligand-induced rearrangement occurs mainly in helices F and G, and the F-F′ - and C-terminal loops. The superimposed structures are: 1TQN, 1WOE, 1WOF, 1WOG, 2JOD, 2VOM, 3NXU, 3TJS, 3UA1, 4I3Q, 4I4G, 4I4H, 4K9T, 4K9U, 4K9V, 4K9W and 4K9X. To simplify viewing, all ligands were excluded from the active site. (**b**) A closer view at the F-F′-G′-G-helical region that serves as a binding site for progesterone (shown in cpk representation). The hydrophobic pocket is thought to represent a peripheral docking site involved in effector/substrate recognition and could play a role in modulating cooperativity [77]